The Impact of ENSO on Extratropical Low Frequency Noise in Seasonal Forecasts

Siegfried D. Schubert, Max J. Suarez, Yehui Chang
Goddard Laboratory for Atmospheres
Greenbelt, Maryland

and

Grant Branstator
National Center for Atmospheric Research
Boulder, Colorado

29 February, 2000

To be submitted to J. Climate

Abstract

This study examines the uncertainty in forecasts of the January-February-March (JFM) mean extratropical circulation, and how that uncertainty is modulated by the El Niño/Southern Oscillation (ENSO). The analysis is based on ensembles of hindcasts made with an Atmospheric General Circulation Model (AGCM) forced with sea surface temperatures observed during the 1983 El Niño and 1989 La Niña events. The AGCM produces pronounced interannual differences in the magnitude of the extratropical seasonal mean noise (intra-ensemble variability). The North Pacific, in particular, shows extensive regions where the 1989 seasonal mean noise kinetic energy (SKE), which is dominated by a "PNA-like" spatial structure, is more than twice that of the 1983 forecasts. The larger SKE in 1989 is associated with a larger than normal barotropic conversion of kinetic energy from the mean Pacific jet to the seasonal mean noise. The generation of SKE due to sub-monthly transients also shows substantial interannual differences, though these are much smaller than the differences in the mean flow conversions. An analysis of the generation of monthly mean noise kinetic energy (MKE) and its variability suggests that the seasonal mean noise is predominantly a statistical residue of variability resulting from dynamical processes operating on monthly and shorter times scales.

A stochastically-forced barotropic model (linearized about the AGCM's 1983 and 1989 base states) is used to further assess the role of the basic state, submonthly transients, and tropical forcing, in modulating the uncertainties in the seasonal AGCM forecasts. When forced globally with spatially-white noise, the linear model generates much larger variance for the 1989 base state, consistent with the AGCM results. The extratropical variability for the 1989 base state is dominanted by a single eigenmode, and is strongly coupled with forcing over tropical western Pacific and the Indian Ocean, again consistent with the AGCM results. Linear calculations that include forcing from the AGCM variance of the tropical forcing and submonthly transients show a small impact on the variability over the Pacific/North American region compared with that of the base state differences.

1. Introduction

It is now well understood that, for the seasonal prediction problem, the mean response of the atmosphere to anomalous boundary forcing is but one aspect of a more general stochastic solution that includes various higher order moments that define a probability density function (PDF, e.g. Barnett 1995; Kumar and Hoerling 1995, Kumar et al. 2000). At the seasonal time scale, the uncertainties due to initial condition errors have saturated in the sense that the statistics associated with planetary and synoptic scale systems have for the most part lost all memory of the initial conditions. Nevertheless, the saturated statistics can be influenced or modulated by slowly varying boundary forcing such as anomalous seas surface temperatures (SSTs). In this study, we examine how tropical SST anomalies associated with ENSO impact the uncertainty of extratropical seasonal forecasts made with an atmospheric general circulation model (AGCM).

The impact of the tropical SST anomalies on the uncertainty of the extratropical response can be direct, for example as a result of changes in variability (uncertainty) of the tropical forcing, or indirect, through changes in the basic state or the variability of subseasonal transients. It is already well established that transients play an important role in the mean extratropical response to ENSO (e.g. Kok and Osteegh 1985; Held et al. 1989). Several recent studies have focused on how the transients are influenced by and feed back on the forced ENSO response. For example, Branstator (1995) emphasize the role of selective feedbacks between the transients and forced response. Chen and Van den Dool (1997) examine how ENSO impacts subseasonal low frequency variability over the North Pacific, and show that both blocking and deep trough flows develop twice as often over the North Pacific during La Nina as compared with El Nino winters. They further show that the difference in magnitude of the low frequency variability is the result of increased energy extraction by the low frequency transients from the mean flow and an enhanced role of high latitude high frequency transients in developing and maintaining blocked flows during La Nina winters.

Kumar et al. (2000) employed ensembles of AGCM simulations forced with observed SSTs for the period 1950-94 for four different models to investigate the impact of SST forcing on the second moment statistics or spread. They find, based on a composite of all warm and cold events, a significant but small reduction in spread over the North Pacific during the warm events and little impact on the spread during cold events. They further suggest that the contribution to seasonal predictability from changes in spread are small compared to the impact of the SST on the mean. Sardeshmuhk et al. (2000) analyzed very

large ensembles of seasonal mean (JFM) forecasts generated with the National Centers for Environmental Prediction (NCEP) AGCM for neutral, warm (1987) and cold (1989) ENSO conditions. They found that the geopotential height response is, in general, more variable for the 1987 SST than for the 1989 SST, though both the warm and cold experiments showed increased variability over the North Pacific compared with the neutral ENSO conditions. They speculate that the increased variability in the geopotential height response for 1987 is in part due to increased variability in rainfall in the central equatorial Pacific.

In this study we examine the role of ENSO in modulating the noise (intra-ensemble variance) of boreal winter forecasts for two cases: the 1983 warm event and the 1989 cold event. We take a case study approach to help isolate the dominant controls on the variability during extreme events, and to avoid averaging different ENSO events that can have quite different atmospheric teleconnection characteristics (e.g. Palmer and Mansfield 1986). We examine the role of the background state, and interannual changes in the intra-ensemble variance of the tropical forcing and middle latitude transients. The study utilizes ensembles of hindcasts with an early version of the Goddard Earth Observing System (GEOS-2) AGCM. The AGCM results are diagnosed within a kinetic energy framework, and with the aid of a stochastically-forced barotropic model linearized about the AGCM ensemble mean states.

Section 2 gives an overview of the AGCM and forecast experiments. The AGCM results are presented in section 3. The results of the stochastically-forced barotropic model linearized about the AGCM ensemble mean flow are presented in section 4. The summary and conclusions are given in section 5.

2. The Model and Forecast Experiments

The AGCM is an early version of the Goddard Earth Observing System (GEOS-2) model described in (Chang et al. 2000). It has 43 sigma levels extending up to 10mb and a horizontal resolution of 2° latitude by 2.5° longitude. The mean ENSO response of this model is described in Chang et al. (2000) based on an ensemble of nine forecasts starting in mid-December for each winter season (JFM) for the period 1980/81 through 1994/95. The results of that study suggest that the ENSO response in the GEOS-2 model tends to be weak. In fact, a comparison of the ENSO response in a number of different models (Shukla et al. 2000) shows a wide range of signal to noise ratios over the Pacific/North

American region. The issue of model dependence and its potential impact on the results of this study is addressed in the conclusions.

Ensembles of 5-10 members, typical of many previous AGCM experiments focusing on the ensemble mean response, are likely too small to obtain reliable higher moment statistics. In this study, we generate ensembles with 27 members to provide more reliable estimates of the second moment statistics. The issue of statistical significance will be discussed in the next section. The initial conditions are based on the GEOS-1 reanalysis (Schubert et al. 1993). The 27 perturbations to the initial conditions are generated by taking the difference between two randomly chosen December states separated by twelve hours, and adding that difference to the 15 December (1982 or 1988) base state (see Schubert and Suarez 1989).

In all AGCM experiments described here, the SST and sea ice are prescribed using observed monthly boundary conditions (Reynolds and Marsico 1993). Soil moisture is prescribed as described in Chang et al. (2000).

3. AGCM Results

As described in Quiroz (1983), the warm event of 1982/83 was one of the strongest El Nino episodes of the century with the lowest recorded value of the Southern Oscillation index (3.5 standard deviations below normal) since 1935, and December – February (DJF) sea surface temperature anomalies exceeding 3°C over much of the eastern equatorial Pacific. The wintertime Northern extratropics were characterized by an unusually deep Aleutian Low, an enhanced and eastward extended Pacific jet, and a positive height anomaly over the Atlantic-Eurasian sector. Cyclone tracks and the jet over the Pacific and United States were south of their normal position, while major wintertime blocking episodes were confined to the Atlantic and European sectors.

The cold event during DJF of 1988/89 was characterized by SSTs of more than 1 degree below normal throughout the central and eastern equatorial Pacific (e.g. Arkin 1989). Large positive height anomalies (exceeding 120m) occurred over the eastern North Pacific acting to divert weather systems to the north of their usual tracks. The east Pacific anomaly was part of a larger scale anomaly pattern consisting of above normal heights at 500mb in the middle latitudes and below normal heights over the poles in both the northern and southern hemispheres. Considerable month-to-month variability occurred over the United States with near normal temperatures in December, very warm in January and very cold in February.

The mean circulation anomalies for January through March (JFM) of 1983 and 1989 are depicted in Figures 1a and 1b in terms of selected isolines of streamfunction or streamlines of the 200mb non-divergent wind. The heavy lines are the observed values from the GEOS-1 reanalysis. The thin lines are from the 27 model hindcasts. Both the observations and model JFM hindcasts show the large differences during these two events over the eastern North Pacific discussed above and reflected here in the largely zonal flow extending across the Pacific into the western United States during the warm event, and the strongly diffluent flow during the cold event.

Another major difference between the two events is in the AGCM's intra-ensemble spread in the streamlines. The 1983 warm event shows a close packing of the JFM streamlines over the central and eastern North Pacific, while for the 1989 cold event there is considerable intraensemble spread. This indicates a substantially greater uncertainty in the hindcasts of the cold event in the diffluent regions of the North Pacific. Over the North Atlantic, there is some tendency for the flow to be more diffluent and the uncertainty to be larger during 1983. The observed JFM streamlines lie near the edge of the model's range of outcomes reflecting the model's tendency to produce a weaker than observed response to the SST anomalies (Chang et al. 2000).

Figures 1c and 1d shows the dominant EOFs of the seasonal mean noise or intra-ensemble variability in the 200mb stream function for 1983 and 1989, respectively. The dominant EOF in 1983 has a strong component in the North Atlantic sector reflecting the somewhat larger variance in that region compared with the Pacific during this year. This mode explains 30% of the intra-ensemble variance. The north/south dipole at high latitudes and the zonally-elongated structure of the EOF are features that bear some resemblance to the western North Atlantic pattern found in the observations on monthly and longer time scales (Wallace and Gutzler 1981). In the Pacific the EOF also shows a north/south structure and zonally-elongated anomalies. We note that the second EOF shows astructure which resembles the Pacific/North American (PNA) pattern (Wallace and Gutzler 1981). During 1989, the dominant EOF of the intra-ensemble variance of the JFM mean stream function shows a well-defined PNA structure. This mode explains 38% of the intra-ensemble variance.

The test for determining the statistical significance of the differences in the intra-ensemble variability between the two years is based on the F-distribution (e.g. DeGroot 1975). With 27 ensemble members, and under the null hypothesis that the variances for 1983 and 1989

are the same, the ratio of the unbiased variance estimates has an F(26,26)-distribution. The ratio of the 1989 to 1983 total intra-ensemble variances (Figures 1c and 1d) shows clearly that the significant extratropical differences in variability between the two years are largely due to the greater variability of the PNA mode during 1989. We note that the region of enhanced variability over the North Atlantic during 1983 is only marginally significant.

We next take a brief look at the variance of the subseasonal transients, how it compares with the observed variance, and its intra-ensemble variability. As we shall see, it is the latter that potentially impacts the interannual differences in the seasonal noise. Figure 2 compares the observed and AGCM submonthly variability of the 200mb stream function. Variability on time scales longer than one month but shorter than one season does not contribute significantly to the kinetic energy conversion terms (see below), so we do not include it here. The AGCM results are the average variances from all 27 ensemble members, while the observations are of course from a single realization. Both the model and observations show substantial differences in the submonthly variability over the eastern North Pacific and western North America. During 1983, the highest variability occurs in a narrow latitudinal band extending across the Pacific into North America, while during 1989 the region of high variability has a greater latitudinal range, extending well north of 60°N. Both the model and observations show a tendency for greater variability in the North Atlantic in 1983, though in the observations the region of maximum variability lies farther to the north. In the model, the largest variability occurs in 1989 in Pacific storm track between Japan and Hawaii, and over the western United States. We note that both the model and observations show higher submonthly variability during 1989 extending southward into the tropics throughout the eastern Pacific (not shown), suggesting greater propagation into the tropics during this year.

It is difficult to determine whether the differences in submonthly variability between the model and observations reflects sampling errors or model errors. Many of the localized features are likely due to sampling differences. That is, the noiser structure in the observations likely reflects the occurrence of just a few events during JFM, while the model results include transients from 27 different JFM realizations. For example, the large but localized region of submonthly variability observed over the North Atlantic during 1983 is not evident in the average statistics from the AGCM. To help sort out these differences we plot in Figure 3 the intra-ensemble standard deviation of the AGCM submonthly variance. Large intra-ensemble variability of the submonthly variability occurs over much of the North Pacific and west coast of the United States during 1989, suggesting that the differences with the observations in this region are likely due to sampling errors. The intra-

ensemble variability of the submonthly variability tends to be smaller during 1983, however, the region of large discrepancy between model and observations in the North Atlantic does tend to be a region of enhanced intra-ensemble variability.

In the following, we examine the nature of the interannual differences in the JFM noise variance using a kinetic energy framework. The ensemble mean seasonal mean noise kinetic energy (SKE) or intra-ensemble variability is defined as

$$SKE = 1/2\left\langle \overline{u}^{*2} + \overline{v}^{*2} \right\rangle, \tag{1}$$

where the star denotes a deviation from the ensemble mean, the angle bracket denotes an ensemble mean, the overbar is a seasonal (JFM) mean, and u and v are the zonal and meridional wind components. Figure 4 shows the interannual differences in SKE. Consistent with Figure 1, pronounced interannual differences in SKE occur over the North Pacific, with 2 to 3 times more SKE during 1989. The reverse is true over the North Atlantic although the differences between the two years are smaller, and the overall magnitudes are considerably less than the 1989 North Pacific values.

The local barotropic conversion terms (e.g. Simmons et al. 1983) in the equation governing the SKE are approximately:

$$C1 = -\left\langle \overline{u}^{*2} - \overline{v}^{*2} \right\rangle \frac{\partial \langle \overline{u} \rangle}{\partial x} - \left\langle \overline{u}^{*} \overline{v}^{*} \right\rangle \frac{\partial \langle \overline{u} \rangle}{\partial y} - \left\langle \overline{u}^{*} \overline{v}^{*} \right\rangle \frac{\partial \langle \overline{v} \rangle}{\partial x} \approx E \bullet \nabla \langle \overline{u} \rangle, \tag{2a}$$

and

$$C2 = \left\langle \left(\overline{u'^2} - \overline{v'^2} \right)^{*} \frac{\partial \overline{u}^{*}}{\partial x} \right\rangle + \left\langle \overline{u'v'}^{*} \frac{\partial \overline{u}^{*}}{\partial y} \right\rangle + \left\langle \overline{u'v'}^{*} \frac{\partial \overline{v}^{*}}{\partial x} \right\rangle. \tag{2b}$$

Here, the prime denotes a deviation from the seasonal mean, and the star and overbar are as in (1) above. C1 is the conversion of kinetic energy from the ensemble mean flow to the SKE, and C2 is the conversion of kinetic energy from the subseasonal transients to the SKE. We will also refer to C1 as the generation of SKE due to the mean flow, and C2 as the generation of SKE due to the subseasonal transients. The approximate form of C1 in (2a) is obtained by dropping the term involving the zonal gradient in the mean meridional wind, which tends to be small (Simmons et al. 1983). The E-vector (Hoskins et al. 1983) is defined here for the seasonal mean intra-ensemble anomalies as

$$E = -\left\langle \overline{u}^{*2} - \overline{v}^{*2} \right\rangle i - \left\langle \overline{u}^{*} \overline{v}^{*} \right\rangle j . \qquad (3)$$

From the simplified form of C1 it is clear that when the E vectors point in the direction of the gradient of the mean zonal wind there is a growth of SKE. In the case of C2, the generation of SKE occurs if the E vectors of the subseasonal transients (not shown) tend to point in a direction opposite to the gradient of the seasonal mean zonal wind anomalies

Figures 5a and 5b show the E-vectors of the seasonal mean noise (3) superimposed on the ensemble mean 200mb zonal winds for 1983 and 1989, respectively. During 1983 the Pacific jet (winds greater than 30m/s) extends eastward across North America to connect with the Atlantic jet. In contrast, during 1989 the Pacific jet is retracted westward with enhanced winds just off the east Asian coast resulting in strong zonal gradients in the zonal wind in the central Pacific. Also, in 1989 the Altantic jet is weaker and shifted to the north compared to 1983. In both years, the E-vectors are directed towards increasing zonal wind in the Pacific jet exit region, indicating a generation of SKE due to the mean flow. Larger E-vectors during 1989, together with the stronger zonal wind gradients associated with the retracted Pacific jet, result in a much larger generation of SKE during 1989 (Fig. 5d). In the Atlantic sector, the larger generation of SKE occurs during 1983 in association with the stronger Atlantic jet during that year (Fig. 5c).

The generation of SKE due to the subseasonal transients (term C2) is shown in Figure 6. We consider only the submonthly transients (Figures 6a and 6b), because the contribution from transients with time scales between one month and one season (not shown) is small. C2 tends to be positive and largest in the jet exit regions and over the eastern oceans. Compared with C1, these conversion terms tend to be small. It is noteworthy, however, that the maxima in C2 tend to occur further to the east. Figures 6c and 6d show the contribution to C2 by weather systems alone (time scales less than 10 days). The strong resemblance to the contribution from the full submonthly variations, suggests that much of the conversion is accomplished by the short period (weather) transients. The main exception is in the Gulf of Alaska where variability with time scales longer than 10 days provides the greatest contribution to the kinetic energy conversion.

While the above results suggest that barotropic conversion from the mean flow is an important source of SKE, it is possible that the noise is generated on shorter time scales (e.g. monthly), and that the seasonal noise is largely a statistical residual of subseasonal

variability. In order to address this question we compare the variance of the seasonal mean noise to the monthly mean noise. If each seasonal mean is considered as an average of three monthly means that are uncorrelated, the variance of the seasonal means is just one third of the variance of the monthly means. In that case, with an ensemble size of 27, the ratio of the variance of the seasonal means to one third the variance of the monthly means has an F(26,78) distribution. This is, however, only approximately true because the F test does not strictly apply here since the numerator and denominator are computed from the same data and are not independent. To circumvent this problem, the quantiles are actually obtained empirically using 10000 realizations of 27x3 unit normals to generate the variances ratios. Values of the ratio greater than 1.4 (1.55) indicate at the 5% (1%) level that the variance of the seasonal means is significantly larger than would be expected for uncorrelated monthly means. Figure 7 shows the ratio of the kinetic energy of the seasonal means to 1/3 of the kinetic energy of the monthly means. The ratio exceeds 1.4 in only a few locations indicating that much of the seasonal mean variance can be explained as a statistical residual of variability occurring at monthly and shorter time scales. We note that the areas with kinetic energy ratios exceeding 1.4 tend to occur in the regions of maximum spatial gradient of the dominant streamfunction EOFs shown in Figure 1.

The implication of the above results is that the underlying dynamical processes generating the noise variance are acting, not on seasonal time scales but, on monthly and shorter time scales. The time scales associated with the barotropic generation from the mean flow in linear calculations is rather sensitive to the basic state (e.g. Simmons et al. 1983; Borges and Sardeshmuhk, 1995; section 4). Observations show that the barotropic generation from the mean flow tends to be positive for anomalies with time scales as short as 20 days, though the efficiency of the conversion is greater for lower frequency modes (Schubert 1986). Also, non-modal growth of decaying normal modes can lead to large energy increases over short time intervals (Borges and Sardeshmuhk, 1995; Sardeshmukh et al. 1997). While it is beyond the scope of this paper to determine the dominant time scales of low frequency variability (see also Feldstein 1999), our point here is that understanding the nature of the seasonal noise requires understanding dynamical processes that generate variability on time scales substantially shorter than one season. Figure 8 shows, for example, the generation of monthly mean noise kinetic energy (MKE) due to energy conversion from the submonthly transients and the mean flow. The results are, to a large extent, similar to those found for the SKE. The generation of MKE from the mean flow over the North Pacific is much larger during 1989 than during 1983. The reverse is true over the North Atlantic. Also, the contribution from the submonthly transients over the

North Atlantic is larger during 1983 compared with 1989, however, this term is again substantially smaller than the conversion from the mean flow.

In addition to dynamical interactions with the basic state and subseasonal transients, extratropical variability is well-kown to be influenced by the tropics on the seasonal time scale (e.g. Palmer 1987). Whether this is important for intra-ensemble variability (in the absence of tropical SST variations) is unclear. A singular value decomposition (SVD, e.g. Bretherton et al. 1992) of the 200mb stream function and precipitation seasonal mean noise (Figure 9) suggests that this may be the case. The dominant SVD mode for 1983 (Figure 9a) shows a strong covariability (48.5% of total squared covariance) between precipitation anomalies in the Indian Ocean and Indonesia (the left singular vector) and a wave train extending across the Pacific and along the west coast of the United States (the right singular vector). In the North Atlantic the mode exhibits a north/south dipole that is in quadrature with the first stream function EOF (Figure 1c). The dominant SVD mode for 1989 (Figure 9b) shows an even stronger covariability (58%) between east/west dipole patterns over India and Indonesia and the PNA pattern (the dominant EOF shown in Figure 1d). The PNA is also associated with substantial precipitation anomalies in the North Pacific. The correlation between the two time series obtained by projecting the 1989 precipitation and streamfunction data onto the dominant left and right singular vectors is quite high (0.96). Therefore, the precipitation mode (left singular vector) explains a substantial fraction (about 35% $=0.96^2$ X 38%) of the variance of the seasonal mean streamfunction noise, though it is likely that this partly reflects the local response of the precipitation to the extratropical PNA circulation anomalies (Figure 9b).

The PNA mode is clearly a robust feature of the 1989 seasonal mean noise, showing up as the dominant mode in both the EOF and the SVD analysis. A structure very similar to the first SVD appears as the dominant mode in a canonical correlation analysis (CCA, not shown). This is noteworthy since, in the CCA, the fields are normalized so that the structures are not influenced by the large inhomogenities in the precipitation distribution (see Figure 13). While the PNA pattern is robust, the nature of the link to tropical precipitation variability is not clear. The vertically-integrated moisture flux associated with this mode (not shown) suggests that a least some of the tropical variability is induced by the extratropical mode as it extends equatorward and influences the tropical divergence. Higgins and Schubert (1996) found a similar coupling between the tropics and North Pacific positive height anomalies on subseasonal time scales in both analyses and model simulations. In particular, they found a substantial feedback to the tropics by the extratropical anomalies during their mature phase. However, that study also found

evidence of a tropical precursor to the development of the extratropical anomalies associated with precipitation anomalies in the western Pacific linked to the Madden Julian Oscillation. In the next section we use a stochastically-forced linear barotropic model to further examine the role of forcing and the basic state in the generation of low frequency noise.

4. Linear Model Results

The linear model (Branstator 1985) is the nondivergent barotropic vorticity equation linearized here about a base state obtained from the GEOS-2 AGCM hindcasts. The model is discretized using spherical harmonics truncated at R15 and steady solutions are directly solved for using matrix operations. The model has second order diffusion with a coefficient of $2.5X10^{-5}$ m^2s^{-1}. There is also Rayleigh friction with a coefficient of $3.86x10^{-6}$, which corresponds to a damping time of 3 days. The damping, while somewhat stronger than typically used, is not inconsistent with data (Klinker and Sardeshmukh 1992).

For the cases presented here, to be consistent with the analysis of the previous section we linearize about the 200mb streamfunction, though the calculations have also been done at 300mb, and all of the conclusions we reach are unchanged. Linear calculations are carried out using the 1983 and 1989 AGCM seasonal mean ensemble mean states, as well as a control state consisting of the average of the 15 years (1980-95) by 9 member ensembles generated previously with the GEOS-2 model (Chang et al. 2000). For later comparison with the linear calculations, Figure 10 shows the global distribution of the 200mb stream function standard deviation (superimposed on the zonal wind) obtained from the AGCM. This shows that, in addition to the variability over the North Atlantic and Pacific Oceans already discussed, considerable variability (also enhanced in 1989) occurs in the jet entrance region of the Pacific jet centered near 70°E.

The linear calculations are performed with a number of different idealized global forcing distributions. Our baseline forcing is white homogeneous noise in space. For any particular solution, the forcing at each gridpoint is found by drawing from a uniform random distribution with values ranging from -1 to 1. We consider two other forcing distributions based on the variance of the AGCM solutions. For these cases, an envelope is applied to the baseline white noise forcing based on the standard deviations of the AGCM's precipitation and submonthly vorticity flux divergence. In all cases, 500

solutions were used to find variances. As described in Dymniikov (1989) and Branstator (1990), the set of solutions with completely unorganized forcing provides information about the role of barotropic dynamics and the climatological mean state in giving structure to low-frequency perturbations. On the other hand, calculations with envelope forcing indicate whether the spatial distribution of the forcing and year to year changes in that distribution affect seasonal perturbations.

Figure 11 shows the standard deviation of the stream function from the linear calculations with the baseline white noise forcing for the 1983, 1989, and the control base states. The control (Figure 11c) shows broad maxima in variance over the North Pacific, North Atlantic and south Asia. These are broadly similar to the regions of high variance found in the AGCM (cf. Figure 10c). The 1983 variance is similar to that of the control in both magnitude and distribution, though there is somwhat less variance over the North Pacific. Consistent with the AGCM results, 1989 (Figure 11b) shows considerably more variance than either 1983 or the control, though the locations of the maxima differ. For example, the large maxima over the North Pacific are shifted further east in the linear model solutions. Also, the high latitude Aleutian maximum is absent from the linear calculations.

The localized nature of the regions of large variance for 1989 suggests the variability for this year might be dominated by a single mode. This is confirmed in Figure 12a which shows the dominant eigenmode. This mode has an e-folding time of 6.6 days (in the absence of damping) and it is stationary. For comparison, the fastest growing mode for the control base state is stationary and has an e-folding time of 16.3 days. For the 1983 base state, it e-folds in 17.6 days and has a period of 2130 days. For the control and 1983 base states, no single mode dominates the variance.

An SVD analysis of the forcing and stream function for 1989 (SVD 1 in Figures 12b and 12c) shows that Indonesia and the Indian Ocean are the regions most responsible for the middle latitude response. SVD 1 explains 19.4% of the covariability. This contrasts with the control and 1983, where the first SVDs (not shown) explain only 8.6 and 8.4% of the covariability, respectively. While differing in details, the linear results for 1989 are similar to the AGCM results (Figure 9b), in that a single perturbation midlatitude structure becomes important over the North Pacific and North America, and the main connection between the forcing and response is the covariability between the dominant eigenmode and the forcing over Indonesia and the Indian Ocean.

The intra-ensemble variance of the AGCM tropical precipitation (Figure 13) shows considerable interannual differences, which may have an influence on the extratropics. For example, more variance occurs in the eastern tropical south Pacific for the warm event (1983), while for 1989 larger variance occurs over the Indian Ocean. To mimic these differences in the AGCM forcing in the linear calculations, we construct families of forcing functions that take into account the three precipitation noise distributions of Figure 13. Using the assumption that tropical precipitation anomalies produce upper tropospheric divergence anomalies of identical horizontal structure and taking into account only the vorticity stretching that would result, we form forcing functions by drawing random numbers and mutiplying them by the standard deviation of precipitation times the coriolis parameter. Poleward of 20 degrees, where the relationship between precipitation anomalies and effective vorticity sources is not readily approximated, forcing is set to zero. Since each of our comparisons of the different base states is restricted to the same type of forcing (e.g. we do not compare envelope to non-envelope forcing), no attempt is made to scale the forcing to make it physically reasonable.

For each year's base state, solutions are computed using the precipitation envelope for that year and the control precipitation envelope. The impact of the precipitation forcing is measured by the ratio of the variances of these two sets of solutions (Figure 14). For 1983, the impact of the precipitation variability is to reduce the response by more than 25% (compared with the control precipitation envelope) over much of the Pacific/North American region. Reduced variability extends across much of the western tropical Pacific and South Pacific. A substantial increase in variability occurs primarily over the eastern tropical Pacific (a factor of 2 locally), with smaller increases over the rest of the tropics, especially over the Indian Ocean. For 1989, the impact of the precipitation variability on the extratropics is largely opposite to that for 1983. An increase in variability of more 25% overs over much of the Pacific/North American region. Reduced variability is largely confined to the central and eastern tropical Pacific (over the cold waters of La Nina) and regions extending polewards and eastwards across the eastern United States and the southern tip of South America.

Figure 15 shows the impact of the basic state in a way that allows us to directly compare the results with the precipitation envelope solutions. In this case, solutions are compared for different base states (each year is compared against the control base state) but, instead of using the global white noise forcing as we did previously in Figure 11, both use the control precipitation envelope. The impact of the 1989 base state (Figure 15b) is much larger than the impact of the 1983 base state (Figure 15a), consistent with our earlier results

with the white noise forcing. The 1989 base state solutions have variability more than a factor 2 larger than the control over a number of regions of the Pacific, North American and the North Atlantic, coinciding with the dominant eigenmode (Figure 12a). For 1983, variance is increased over the North and South Pacific, and much of the Atlantic. Comparison with Figure 14 shows that the impact of the 1989 base state over the Pacific/North American region is much larger than the impact of the differences in the precipitation variability.

We next consider the impact of interannual differences in the AGCM's submonthly transients on the extratropical mean response (Figure 3). In this case, an envelope is applied to the baseline forcing based on the standard deviation of the submonthly vorticity flux divergence (not shown). Specifically, the random numbers are multiplied by the standard deviation of the vorticity flux divergence equatorward of 60°. Comparing the result (Figure 16a) of forcing the 1983 basic state model with forcing distributions based on control and 1983 vorticity flux divergence envelopes, we find the impact in the extratropics is typically less than 30%, with generally reduced variability over the Pacific/North American region. The impact is substantial for the 1983 base state (Figure 16a) only in the eastern tropical Pacific where the impact exceeds 50% (see also Figure 14a). A similar calculation using the 1989 basic state and 1989 vorticity flux distribution indicates (Figure 16b) the change in the variance of vorticity fluxes in that year too may have made a small contribution the midlatitude low-frequency noise found in that year. We note that this does not rule out the possibility that differences in the structure of the transients could be important, though we do not consider that possibility here.

5. Summary and Conclusions

In this study we examined how the uncertainty in extratropical seasonal mean forecasts is impacted by interannual differences in the background state, tropical forcing, and subseasonal transients, associated with the 1983 El Nino and 1989 La Nina events. The analysis was based on two sets (one for each year) of 27 hindcasts generated from 15 December perturbed initial conditions, using the GEOS-2 atmospheric general circulation model (AGCM) and sea surface temperatures (SSTs) specified from observations. The forecast uncertainty or noise was estimated from the intra-ensemble variability of the 27 January-February-March (JFM) mean hindcasts. A stochastically-forced barotropic model linearized about the AGCM's 1983 and 1989 base states was used to further assess the mechanisms modulating the uncertainties in the seasonal forecasts.

The results show that there are pronounced differences in the magnitude of the extratropical seasonal mean noise during these two years. The North Pacific, in particular, shows extensive regions where the 1989 JFM mean noise kinetic energy (SKE) is more than twice that of the 1983 forecasts. These differences in variability are highly significant and reflect the large contribution of the Pacific/North American (PNA) pattern to the noise of the 1989 JFM hindcasts. A diagnostic analysis of the SKE shows that the larger North Pacific values in 1989 are associated with a larger barotropic conversion of kinetic energy from the mean Pacific jet to the seasonal mean noise. During 1983, both the SKE and conversion over the North Atlantic are larger than in 1989. The increased PNA variability and generation of SKE by the mean flow during 1989 are consistent with the results of Chen and Van den Dool (1997). That study showed that blocking and deep trough flows develop twice as often over the North Pacific during La Nina winters compared with El Nino winters. They also found an important contribution to the low frequency variability from high frequency transients (in high latitudes): the current results suggest a minor role for these transients. It is unclear whether these differences represent model deficiencies or whether they are indicative of sampling variability.

As mentioned earlier, the current model has a rather weak ENSO response, and we must question whether that leads to unrealistic noise estimates. Comparisons of the noise in the GEOS-2 AGCM with that of five other AGCMs (Shukla et al. 2000) suggests, however, that that is not the case. In fact, the GEOS-2 noise estimates are comparable to those of several other models with considerably stronger ENSO responses over the Pacific/North American region. Nevertheless, the issue of model dependence is an important concern. Kumar et al. (2000) examined four different AGCMs and found a significant but small decrease in variability over the North Pacific for warm ENSO conditions and little change for cold conditions. That study, however, was based on a composite of all warm and cold events during 1950-94. We suggest that the smaller impact found in that study may be in part the result of compositing events with different seasonal mean extra-tropical responses (e.g. Palmer and Mansfield 1986), and therefore different mean flow kinetic energy conversions. Sardeshmukh et al. (2000), for example, found an increase in variability in the geopotential height response over the North Pacific for both the 1989 cold and 1987 warm event compared with neutral ENSO conditions. Clearly, further work is needed to sort out differences in variability resulting from model differences.

Our analysis of the time scales of the seasonal mean noise suggests that the noise is not generated at these very long (seasonal) time scales, but that it is for the most part statistically indistinguishable from variability that is uncorrelated from one month to the

next. This interpretation of the seasonal mean variaibiltiy as a statistical residue of shorter time scales is further supported by the similarity of the kinetic energy conversions computed from the seasonal and monthly data.

The importance of the differences in the base states in the generation of SKE was confirmed with the linear model. When forced globally with homogeneous, spatially-white noise, the linear model generates variance over the North Pacific for the 1989 base state that is more than a factor of two larger than for the 1983 base state. The 1989 variability is dominated by a single eigenmode, and it is strongly coupled with forcing over the tropical western Pacific and the Indian Ocean. A similar coupling to the tropics is found in the AGCM results, which for 1989 show a strong covariance between the PNA and precipitation anomalies in the western Pacific and Indian Ocean. We note that a number of previous studies have identified perturbations in the western Pacific and Indonesian regions as being particularly efficient at exciting an extratropical response (e.g., Simmons et al. 1983) .

In addition to differences in the base states, the SKE is also potentially impacted by interannual differences in the intra-ensemble noise in the tropical forcing and sub-monthly transients. The impact of the tropical forcing was examined in the linear model by modifying the variance of the global white noise forcing to include an envelope based on the AGCM JFM intra-ensemble precipitation variance equatorward of 20°. The results show a modest impact over the North Pacific and North America, with about a 25% reduction in variance for 1983 and a 25% increase in variance for 1989 compared with the control. The impact of the subseasonal transients was determined by applying an envelope to the white noise forcing based on the variance of the AGCM submonthly vorticity flux divergence equatorward of 60°. These results also show only a modest impact over the North Pacific and North America, with about a 20% reduction in variance for 1983 and a 20% increase in variance for 1989 compared with the control. For both the precipitation and submonthly transients, the greatest impact on the variability is confined to the tropical central and eastern Pacific. We note that Newman et al. (1997) suggest that it is important to include the space-time structure of the forcing to obtain improved barotropic model predictions of the wintertime flow, though that is not considered here.

We conclude that the increased uncertainty in the GEOS-2 AGCM seasonal mean forecasts during 1989 compared with 1983 is largely due to the differences in the basic state. While these results are generally consistent with observations (Chen and Van den Dool 1997), they must be tempered by the fact that there is considerable model dependence in the noise

and signal in seasonal forecasts (e.g. Shukla et al. 2000). Our results further suggest that, in view of the large differences in the extratropical mean response to ENSO events, the analysis of composite events can give a misleading picture of the uncertainties associated with ENSO forecasts. Progress in this area will require more diagnostic studies of individual ENSO events based on ensembles of seasonal forecasts sufficiently large to obtain reliable estimates of second order statistics.

References

Arkin, P., 1989: The global climate for December 1988-February 1989: Cold episode in the tropical Pacific continues. J. Climate, 2, 737-757.

Barnett, T.P., 1995: Monte Carlo climate forecasting, J. Clim. 8, 1005-1022.

Borges, M.D. and Sardeshmuhk, P.D., 1995: Barotropic Rossby wave dynamics of zonally-varying upper-level flows during northern winter. J. Atmos. Sci., 52, 3779-3796.

Branstator, G., 1985: Analysis of general circulation model sea-surface temperature anomaly simulations using a linear model. Part I: Forced solution. J. Atmos. Sci., 42, 2225-2241.

Branstator, G., 1990: Low-frequency patterns induced by stationary waves. J. Atmos. Sci., 47, 629-648.

Branstator, G., 1995: Organization of storm track anomalies by recurring low-frequency circulation anomalies. J. Atmos. Sci., 52, 207-226.

Bretherton, C.S., C. Smith and J.M. Wallace, 1992: An intercomparison of methods for finding coupled patterns in climate data. J. Climate, 5, 541-560.

Chang, Y., S.D. Schubert, M.J. Suarez, 2000: Boreal winter predictions with the GEOS-2 GCM: The role of boundary forcing and initial conditions. Quart. J. Roy. Met. Soc., to appear.

Chen, W. Y., and H.M. Van den Dool, 1997: Asymmetric impact of tropical SST anomalies on atmospheric internal variability over the North Pacific, J. Atmos. Sci., 54, 725-740.

DeGroot, M. H., 1975: Probability and Statistics. Addison-Wesley Publishing Co., Reading, MA, pp 607.

Dymniikov, V.P. and A.N. Filatov, 1989: On problem of stability of quasi-stationary equivalent barotropic atmospheric flows. Soviet J. Num. Anal. Math. Mod., 4, 227-238.

Feldstein, S.B. 1999: Teleconections and ENSO: The timescale,power spectra, and climate noise properties. Submitted to J. Climate.

Held, I.M., S.W. Lyons, and S. Nigam, 1989: Transients and the extratropical response to El Nino. *J. Atmos. Sci.*, 46, 163-174.

Higgins, R. W., and S. D. Schubert, 1996: Simulations of persistent North Pacific circulation anomalies and interhemispheric teleconnections. *J. Atmos. Sci*, 53, 188-207.

Hoskins, B.J., I.N. James, and G.H. White, 1983: The shape propagation and mean flow interaction of large-scale weather systems, J. Atmos.Sci., 40, 1595-1612.

Klinker, E. and P.D. Sardeshmukh, 1992: The diagnosis of mechanical dissipation in the atmosphere from large-scale balance requirements. J. Atmos. Sci., 49, 608-627.

Kok, C.J. and J.D. Opsteegh, 1985: Possible causes of anomalies in seasonal mean circulation patterns during the 1982-83 El Nino event. J. Atmos. Sci., 42, 677-694.

Kumar, A. and M. P. Hoerling, 1995: Prospects and limitations of seasonal atmospheric GCM predictions. Bull. Amer. Meteor. Soc., 76, 335-345.

Kumar, A., A. Barnston, P. Peng, M. Hoerling, L. Goddard, 2000: Changes in the spread of the variability of the seasonal mean atmospheric states associated with ENSO.

Newman, M., P.D. Sardeshmukh, and C. Penland, 1997: Stochastic forcing of the wintertime extratropical flow. J. Atmos. Sci., 54, 435-455.

Palmer, T. N., and D.A. Mansfield, 1986: A study of wintertime circulation anomalies during past El Nino events using a high resolution general circulation model II: Variability of the seasonal mean response. Quart. J. Roy. Meteor. Soc., 112, 639-660.

Palmer, T.N., 1987: Modelling low frequency variability of the atmosphere. Atmosphere and Ocean Variability. H. Cattle, ed., Royal Meteorological Society. 77-103.

Palmer, T.N., 1988: Medium and extended range predictability, stability of the PNA mode, and atmospheric response to sea surface temperature anomalies, Quart. J. Roy. Meteor. Soc., 114, 691-713.

Quiroz, R.S., 1983: The climate of the "El Nino" winter of 1982-83- A season of extraordinary climate anomalies. Mon.Wea.Rev., 111, 1685-1706.

Reynolds, W. R. and D.S. Marsico, 1993: An improved real-time global sea surface temperature analyses. J. Climate, 6, 114-119.

Sardeshmukh, P.D., M. Newman, M.D. Borges, 1997: Free barotropic Rossby wave dynamics of the wintertime low-frequency flow. J. Atmos. Sci., 54, 5-23.

Sardeshmukh, P.D., G.P. Combo and C. Penland, 2000: Changes of probability associated with El Niño. Preprint volume, Eighth Conference on Climate Variations, Denver, Colorado, 13-17 September 1999, 235pp.

Schubert, S.D., 1986: The structure, energetics and evolution of the dominant frequency-dependent three-dimensional atmospheric modes. J. Atmos. Sci., 43, 1210-1237.

Schubert, S. D., and M. J. Suarez, 1989: Dynamical predictability in a simple general circulation model: average error growth. J. Atmos. Sci., 46, 353-370.

Schubert, S.D., R. B. Rood and J. Pfaendtner, 1993: An Assimilated Data Set for Earth Science Applications *Bull. Amer. Meteor. Soc.*, 74, 2331-2342.

Shukla, J., J. Anderson, D. Baumhefner, Y. Chang, E. Kalnay, L. Marx, D. Paolino, S. Schubert, D. Straus, M. Suarez, J. Tribbia, 2000: Dynamical Seasonal Prediction, Bull. Amer. Met. Soc., in review.

Simmons, A.J., J.M. Wallace and G. Branstator, 1983: Barotropic wave propagation and instability, and atmospheric teleconnection patterns. *J. Atmos. Sci.*, 40, 1363-1392.

Wallace, J. M., and D. S. Gutzler, 1981: Teleconnections in the geopotential heighht field during the Northern Hemisphere winter. Mon. Wea. Rev., 109, 784-812.

List of Figures

Figure 1: Three arbitrarily chosen JFM mean streamlines at 200mb for all 27 ensemble members of the AGCM hindcasts (thin dashed lines) and the observations (thick dashed lines) for a) 1983 and b) 1989. The dominant EOF of the 200mb stream function of the AGCM JFM mean noise for c) 1983 and d) 1989. The heavy lines in c) and d) show the ratio of the 1989 JFM noise variance to the 1983 JFM variance. Contour levels show the 10%, 5%, 1% and 0.2% two-sided significant levels (solid lines indicate regions where 1989 variance is larger than 1983 variance, and dashed lines indicate the reverse).

Figure 2: Submonthly variance of the 200mb stream function for JFM computed from the GEOS-1 reanalyses for a) 1983 and b) 1989. The AGCM submonthly JFM variance of the 200mb stream function averaged over the 27 hindcasts for c) 1983 and d) 1989. Units are $(m^2/sX10^6)^2$.

Figure 3: Intra-ensemble standard deviation of the submonthly variance of the 200mb stream function for JFM computed from the 27 AGCM hindcasts for a) 1983 and b) 1989. Units are $(m^2/sX10^6)^2$.

Figure 4: JFM ensemble mean seasonal mean noise kinetic energy (SKE) computed from the 27 AGCM hindcasts for a) 1983 and b) 1989. Units are $(m/s)^2$.

Figure 5: The AGCM ensemble mean JFM 200mb zonal wind with superimposed E-vectors $(m/s)^2$ of the seasonal mean noise at 200mb for a) 1983 and b) 1989, and the mean flow generation term (m^2/s^2/day) for c) 1983 and d) 1989. The contour levels in a) and b) are 10m/s. Values greater than 30m/s are shaded. In c) and d) the heavy contour is a repeat of the 30 m/s contour of the zonal wind field for each year. The light shading indicates values less than -5 m^2/s^2/day, and the dark shading indicates values larger than 20 m^2/s^2/day.

Figure 6: The generation of SKE for 1983 by a) the sub-monthly transients and c) the short period transients (periods< 10 days). b) and d) are the same, but for 1989. Units are $(m/s)^2$/day.

Figure 7: One third of the ensemble mean monthly mean noise kinetic energy at 200mb for a) 1983 and b) 1989. Units are $(m/s)^2$. Values greater than 10 are shaded. The ratio of the

actual to the predicted (1/3 the monthly) ensemble mean seasonal mean noise kinetic energy for c) 1983 and d) 1989. Values less than 0.8 and greater than 1.4 are shaded

Figure 8: Generation of monthly mean noise KE (MKE) for 1983 by a) submonthly transients and c) the mean flow. b) and d) are the same, but for 1989. Units are $(m/s)^2/day$.

Figure 9: The dominant SVD of the JFM mean precipitation and 200mb stream function noise (intra-ensemble variability) for a) 1983 and b) 1989. The percentages are the fraction of the covariability between the precipitation and stream function explained by each mode. Units are arbitrary.

Figure 10: Global distribution of the AGCM JFM ensemble mean 200mb zonal wind (m/s) and the JFM stream function noise (intra-ensemble standard deviation, $m^2/sX10^6$) for a) 1983, b) 1989 and c) 1980-95. The values in c) are based on 9-member ensembles for each year. The 1983 and 1989 values are based on 27 ensemble members.

Figure 11: Standard deviation of the stream function from the linear model solutions with global white noise forcing for a) the 1983 base state, b) the 1989 base state, and c) the control (1980-95) base state. Contour intervals are the same in each panel but arbitrary.

Figure 12: a) The dominant eigenmode of the linear model for the 1989 base state. The dominant SVD of b) the stream function and c) the forcing for the 1989 base state with white noise forcing. Contour intervals are arbitrary.

Figure 13: The global distribution of the AGCM noise (intra-ensemble variance) of the JFM precipitation based on a) the 27 ensemble members for 1983, b) the 27 ensemble members for 1989, and c) the 9-member ensembles covering the period 1980-95. Units are $(mm/day)^2$.

Figure 14: Results from the linear model showing the impact of the AGCM precipitation envelopes applied to the global white noise forcing equatorward of 20°. a) the ratio of the variance of 1983 base state with the 1983 precipitation envelope solutions to the variance of the 1983 base state with the control (1980-95) precipitation envelope solutions. b) the ratio of the variance of 1989 base state with the 1989 precipitation envelope solutions to the variance of the 1989 base state with the control (1980-95) precipitation envelope solutions.

Figure 15: Results from the linear model showing the impact of the AGCM base states. In all runs the AGCM control precipitation envelope is applied to the global white noise forcing equatorward of 20°. See text for details. a) the ratio of the variance of the solutions with the 1983 base state to the variance of the solutions with the control base state. b) the ratio of the variance of the solutions with the 1989 base state to the variance of the solutions with the control base state.

Figure 16: Results from the linear model showing the impact of the AGCM submonthly vorticity flux divergence envelope applied equatorward of 60°. See text for details. a) the ratio of the variance of 1983 base state with the 1983 vorticity flux divergence envelope solutions to the variance of the 1983 base state with the control (1980-95) vorticity flux divergence envelope solutions. b) the ratio of the variance of 1989 base state with the 1989 vorticity flux divergence envelope solutions to the variance of the 1989 base state with the control (1980-95) vorticity flux divergence envelope solutions.

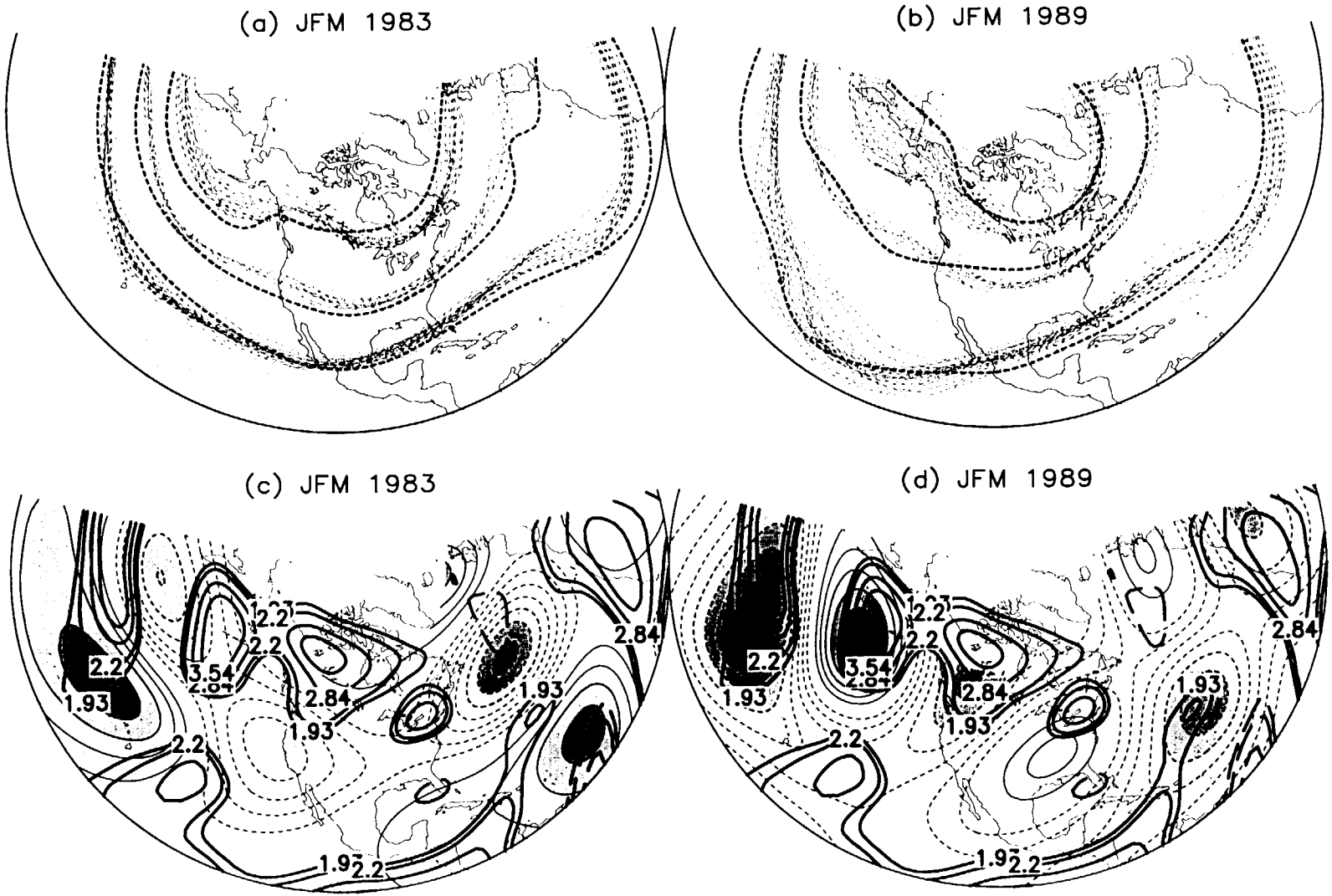

Figure 1: Three arbitrarily chosen JFM mean streamlines at 200mb for all 27 ensemble members of the AGCM hindcasts (thin dashed lines) and the observations (thick dashed lines) for a) 1983 and b) 1989. The dominant EOF of the 200mb stream function of the AGCM JFM mean noise for c) 1983 and d) 1989. The heavy lines in c) and d) show the ratio of the 1989 JFM noise variance to the 1983 JFM variance. Contour levels show the 10%, 5%, 1% and 0.2% two-sided significant levels (solid lines indicate regions where 1989 variance is larger than 1983 variance, and dashed lines indicate the reverse).

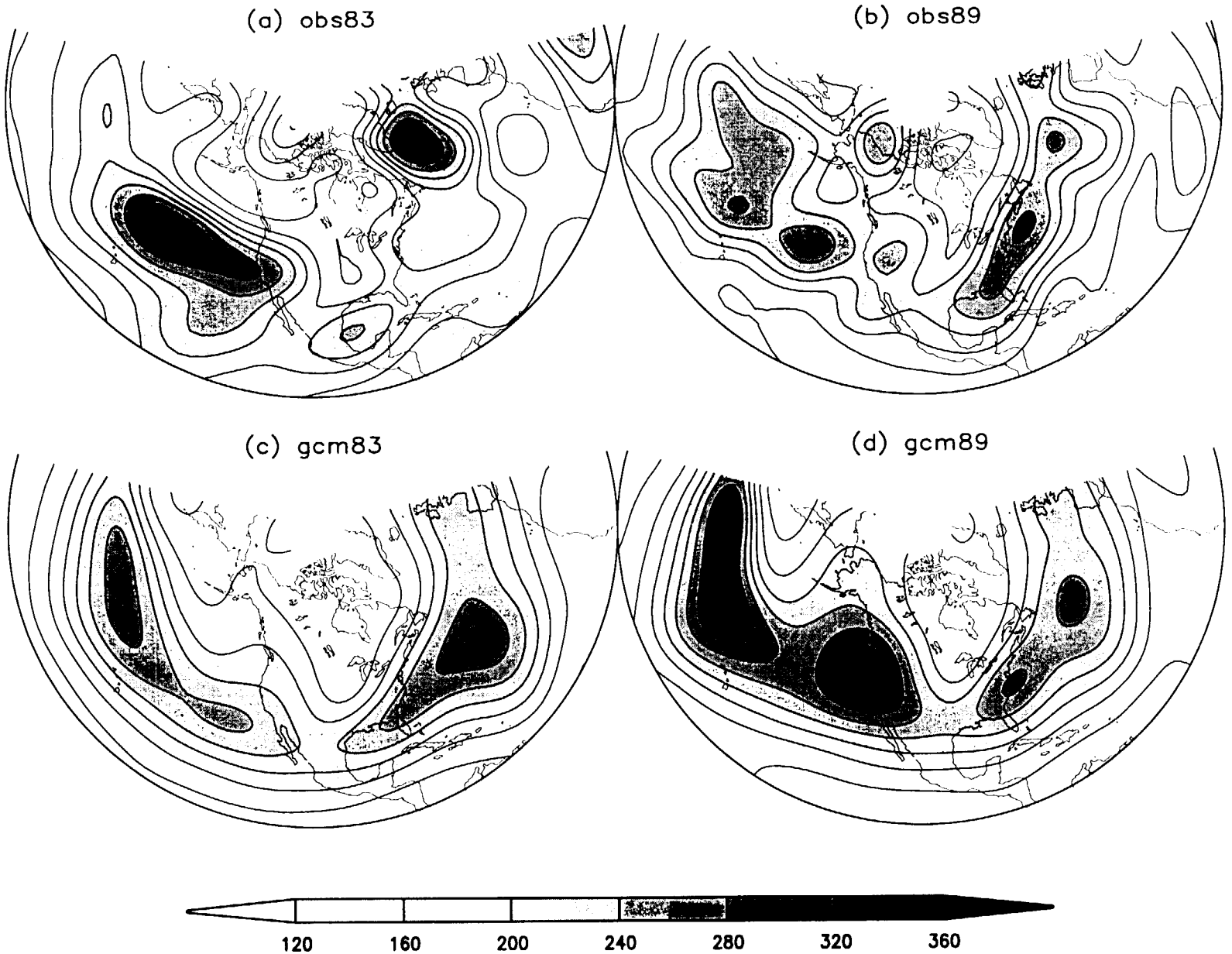

Figure 2: Submonthly variance of the 200mb stream function for JFM computed from the GEOS-1 reanalyses for a) 1983 and b) 1989. The AGCM submonthly JFM variance of the 200mb stream function averaged over the 27 hindcasts for c) 1983 and d) 1989. Units are $(m^2/sX10^6)^2$.

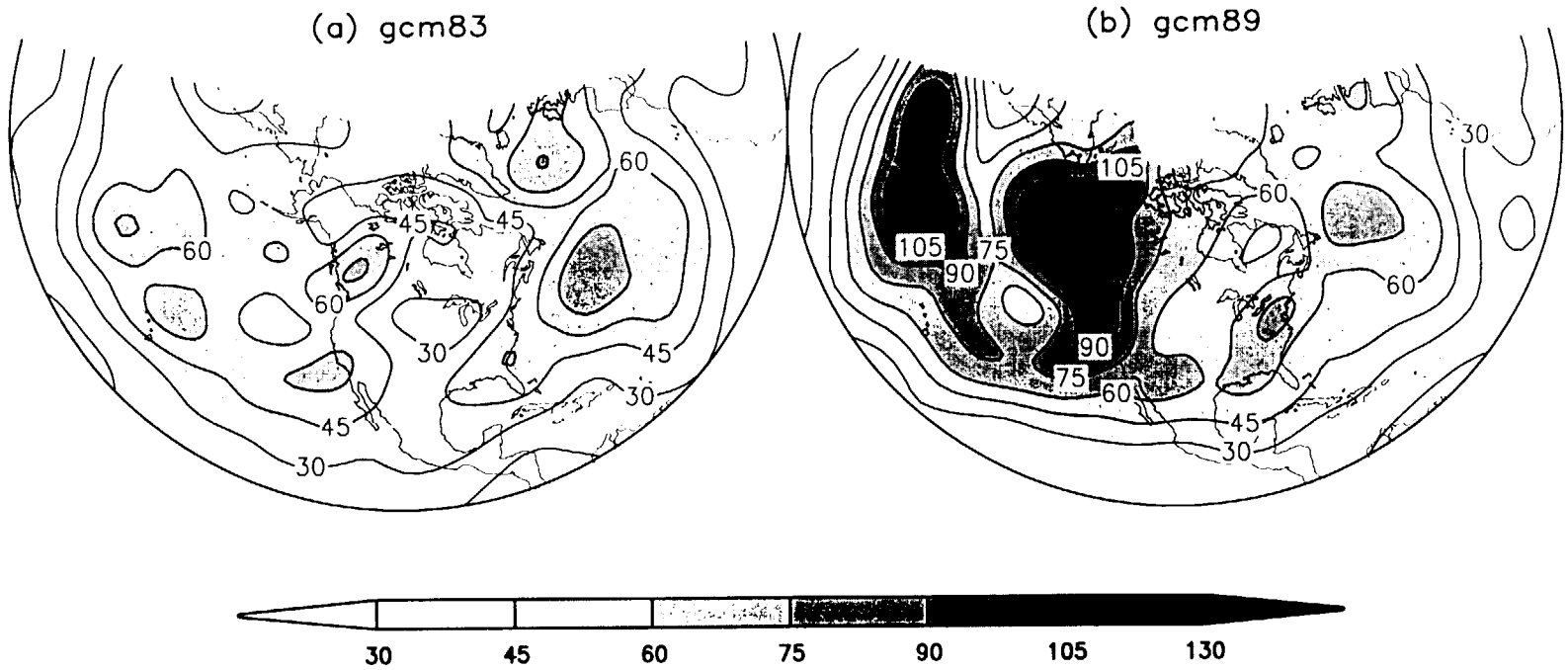

Figure 3: Intra-ensemble standard deviation of the submonthly variance of the 200mb stream function for JFM computed from the 27 AGCM hindcasts for a) 1983 and b) 1989. Units are $(m^2/sX10^6)^2$.

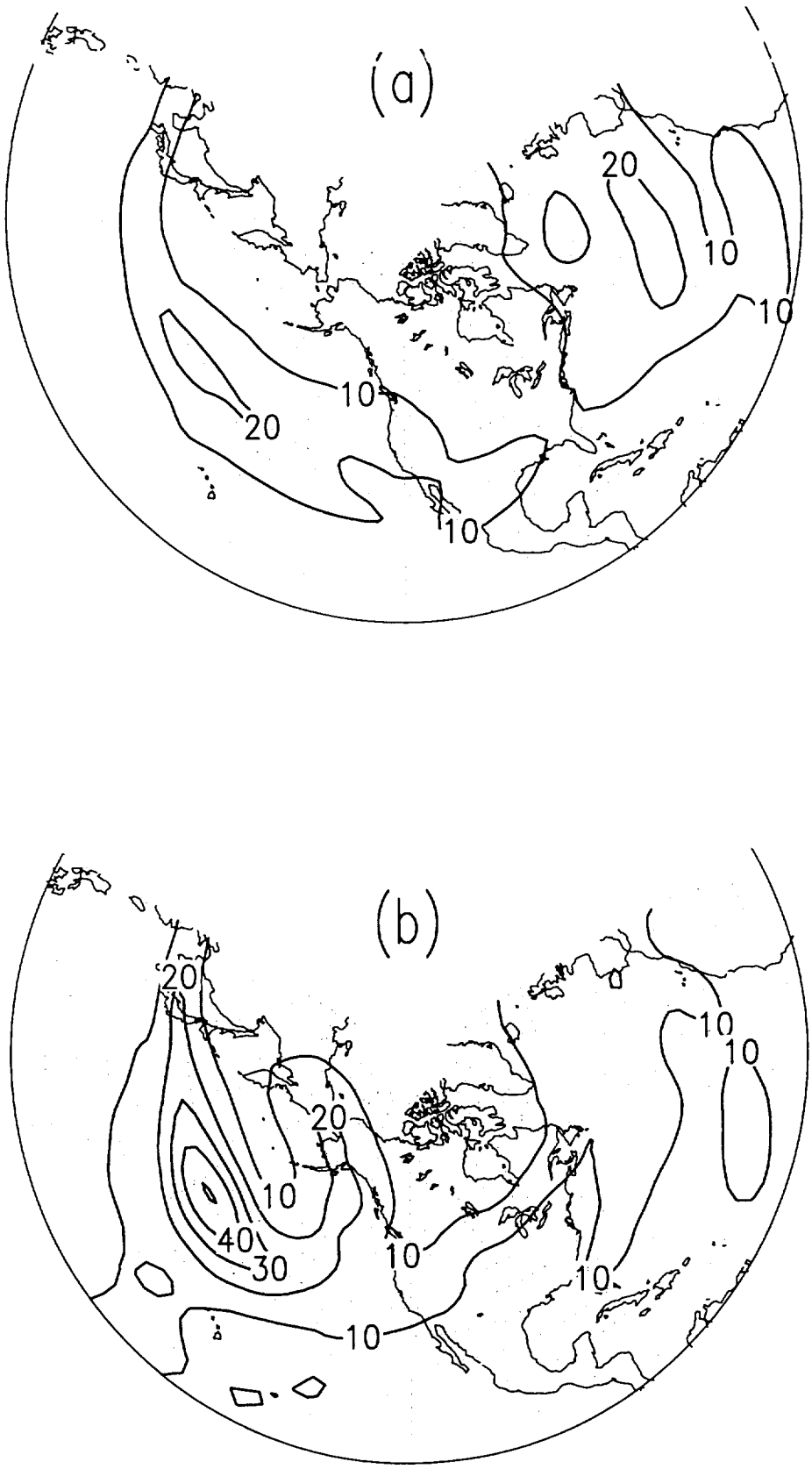

Figure 4: JFM ensemble mean seasonal mean noise kinetic energy (SKE) computed from the 27 AGCM hindcasts for a) 1983 and b) 1989. Units are $(m/s)^2$.

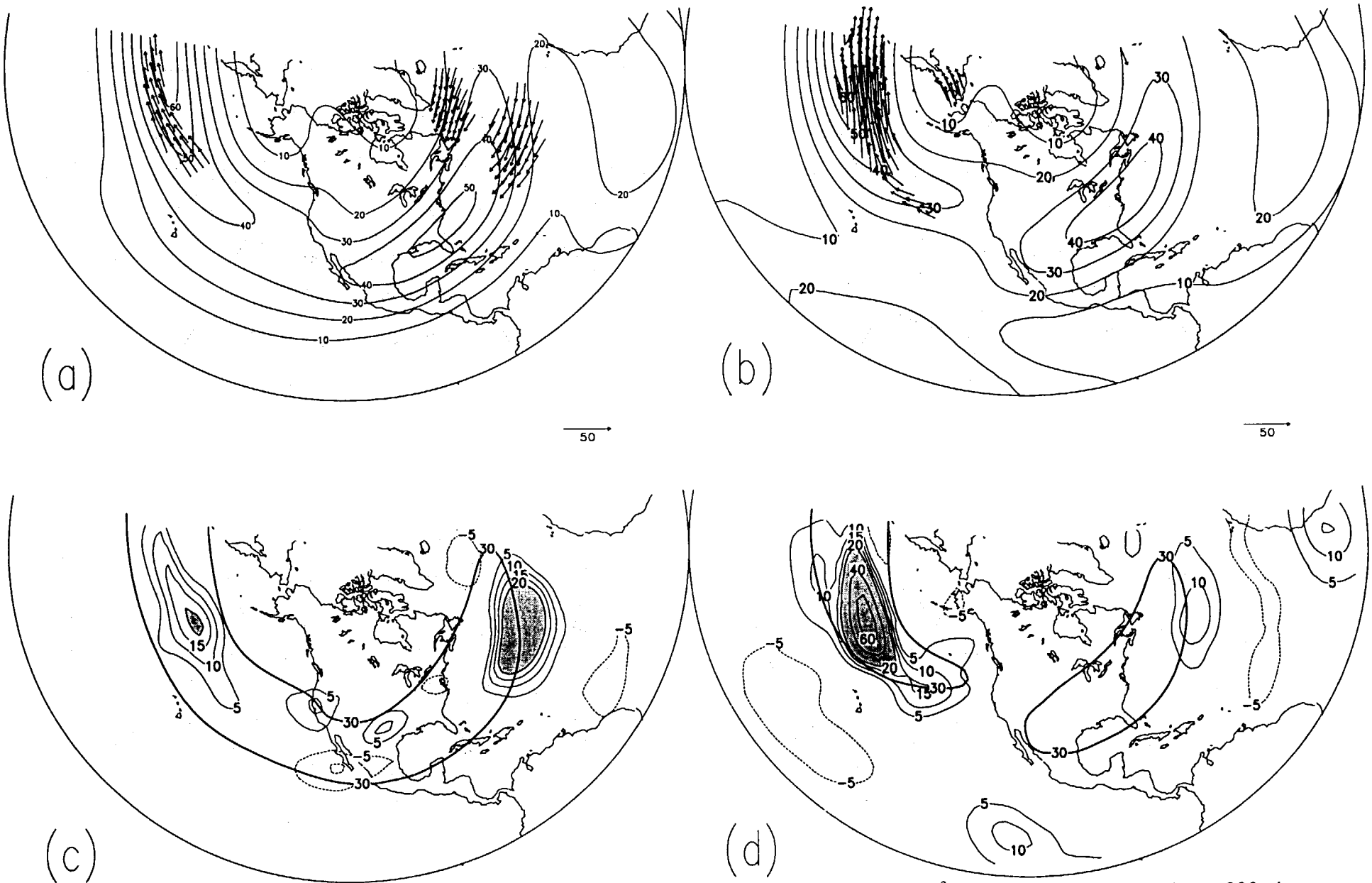

Figure 5: The AGCM ensemble mean JFM 200mb zonal wind with superimposed E-vectors $(m/s)^2$ of the seasonal mean noise at 200mb for a) 1983 and b) 1989, and the mean flow generation term (m^2/s^2/day) for c) 1983 and d) 1989. The contour levels in a) and b) are 10m/s. Values greater than 30m/s are shaded. In c) and d) the heavy contour is a repeat of the 30 m/s contour of the zonal wind field for each year. The light shading indicates values less than -5 m^2/s^2/day, and the dark shading indicates values larger than 20 m^2/s^2/day.

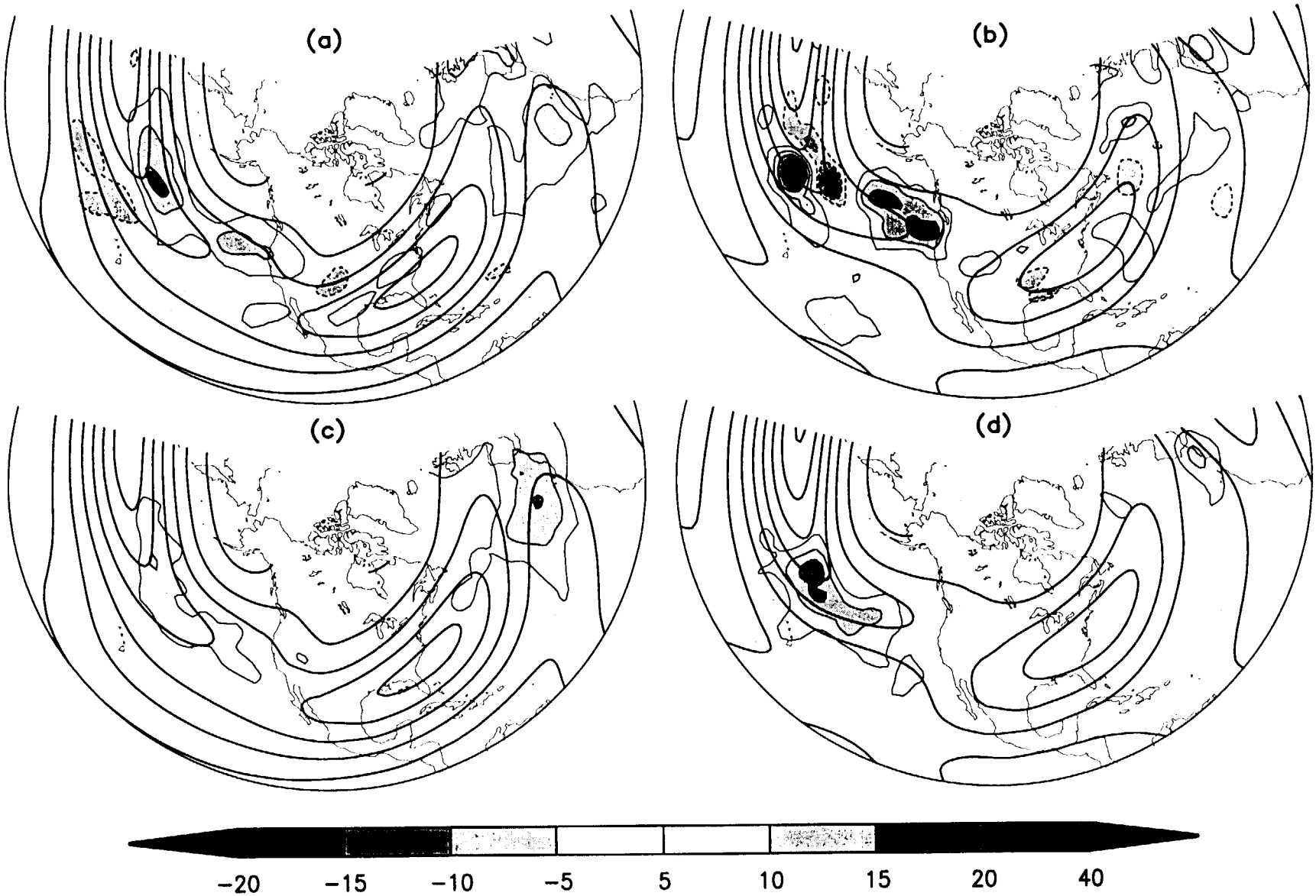

Figure 6: The generation of SKE for 1983 by a) the sub-monthly transients and c) the short period transients (periods< 10 days). b) and d) are the same, but for 1989. Units are $(m/s)^2$/day.

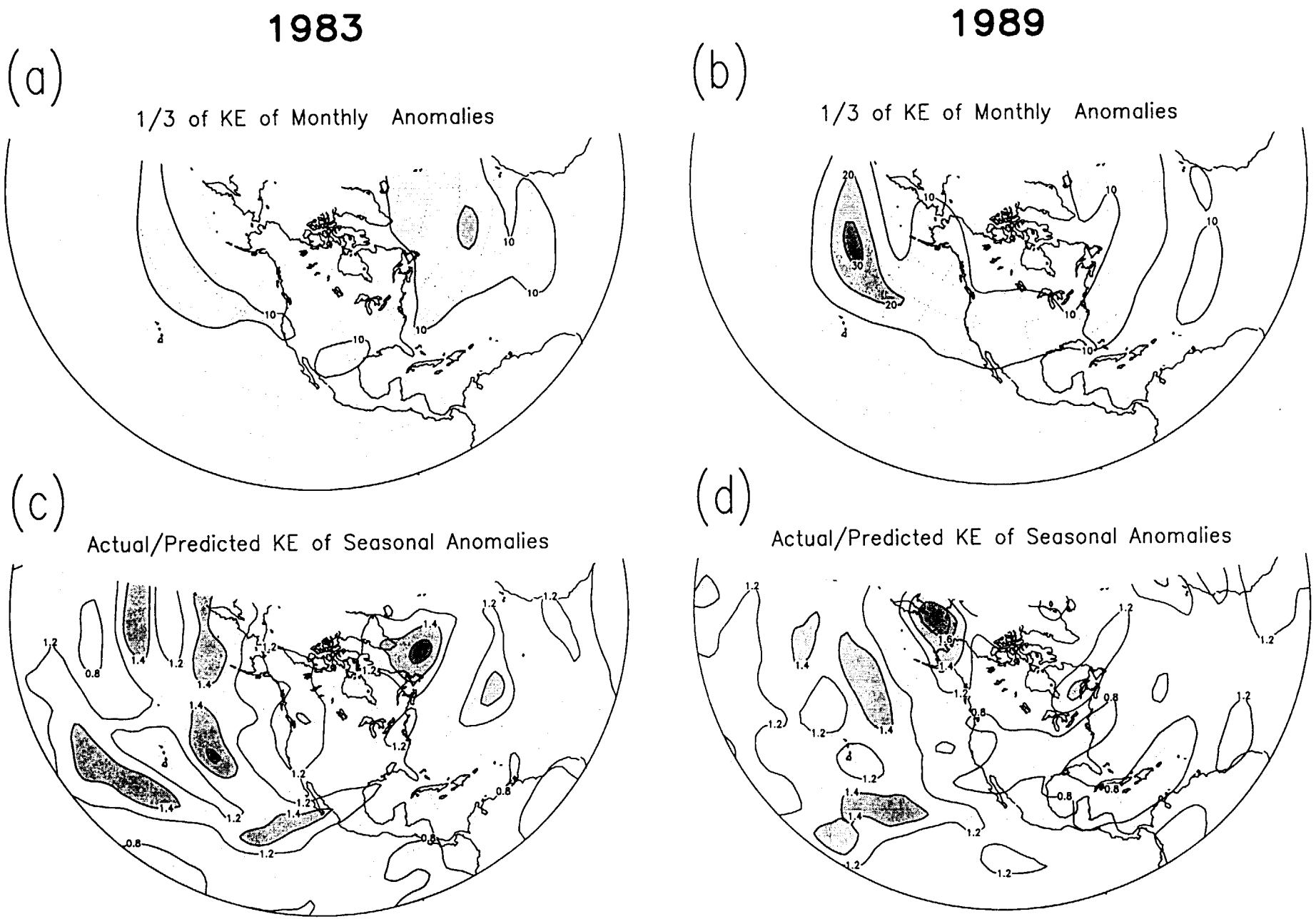

Figure 7: One third of the ensemble mean monthly mean noise kinetic energy at 200mb for a) 1983 and b) 1989. Units are $(m/s)^2$. Values greater than 10 are shaded. The ratio of the actual to the predicted (1/3 the monthly) ensemble mean seasonal mean noise kinetic energy for c) 1983 and d) 1989. Values less than 0.8 and greater than 1.4 are shaded

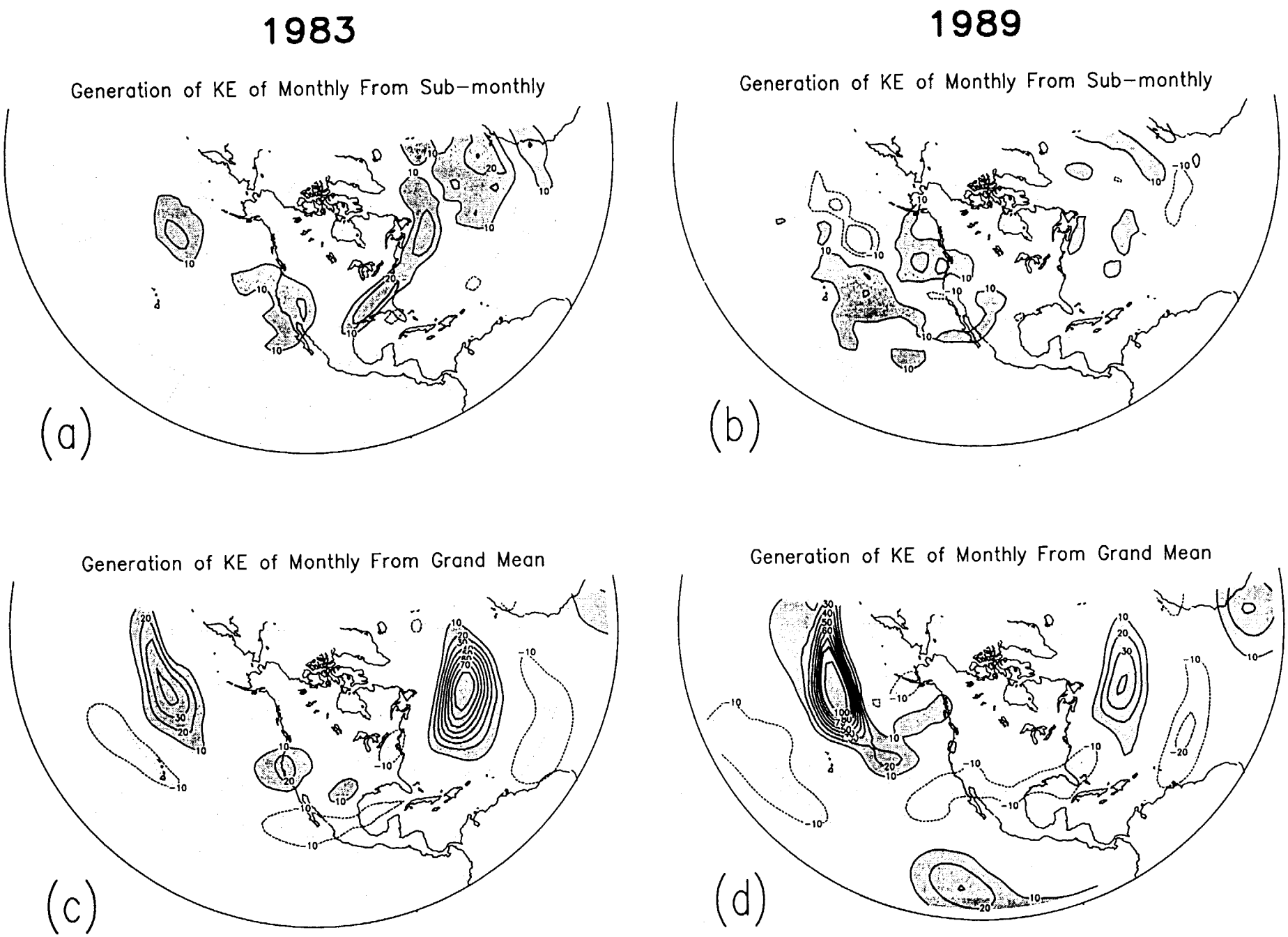

Figure 8: Generation of monthly mean noise KE (MKE) for 1983 by a) submonthly transients and c) the mean flow. b) and d) are the same, but for 1989. Units are $(m/s)^2$/day.

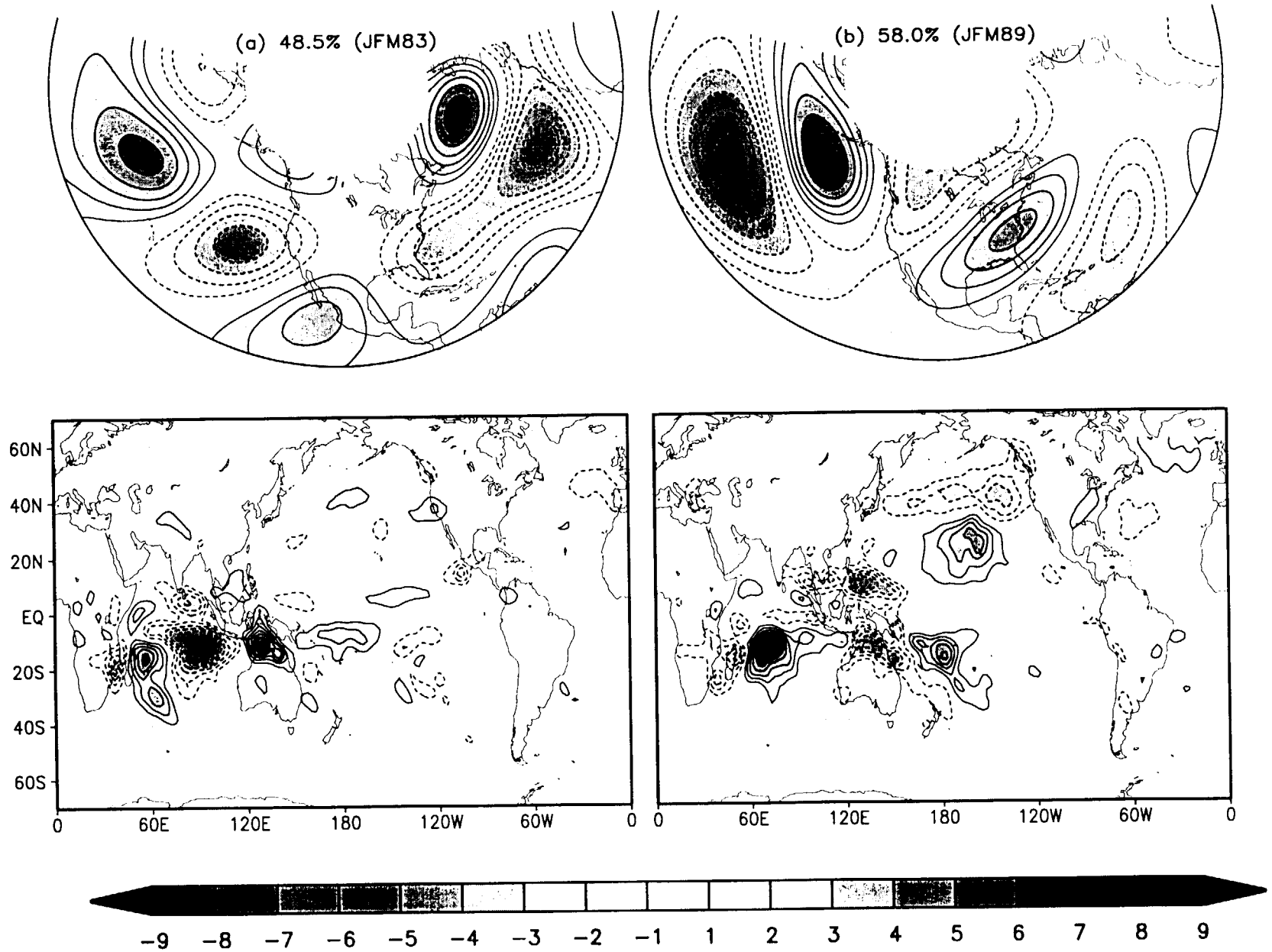

Figure 9: The dominant SVD of the JFM mean precipitation and 200mb stream function noise (intra-ensemble variability) for a) 1983 and b) 1989. The percentages are the fraction of the covariability between the precipitation and stream function explained by each mode. Units are arbitrary.

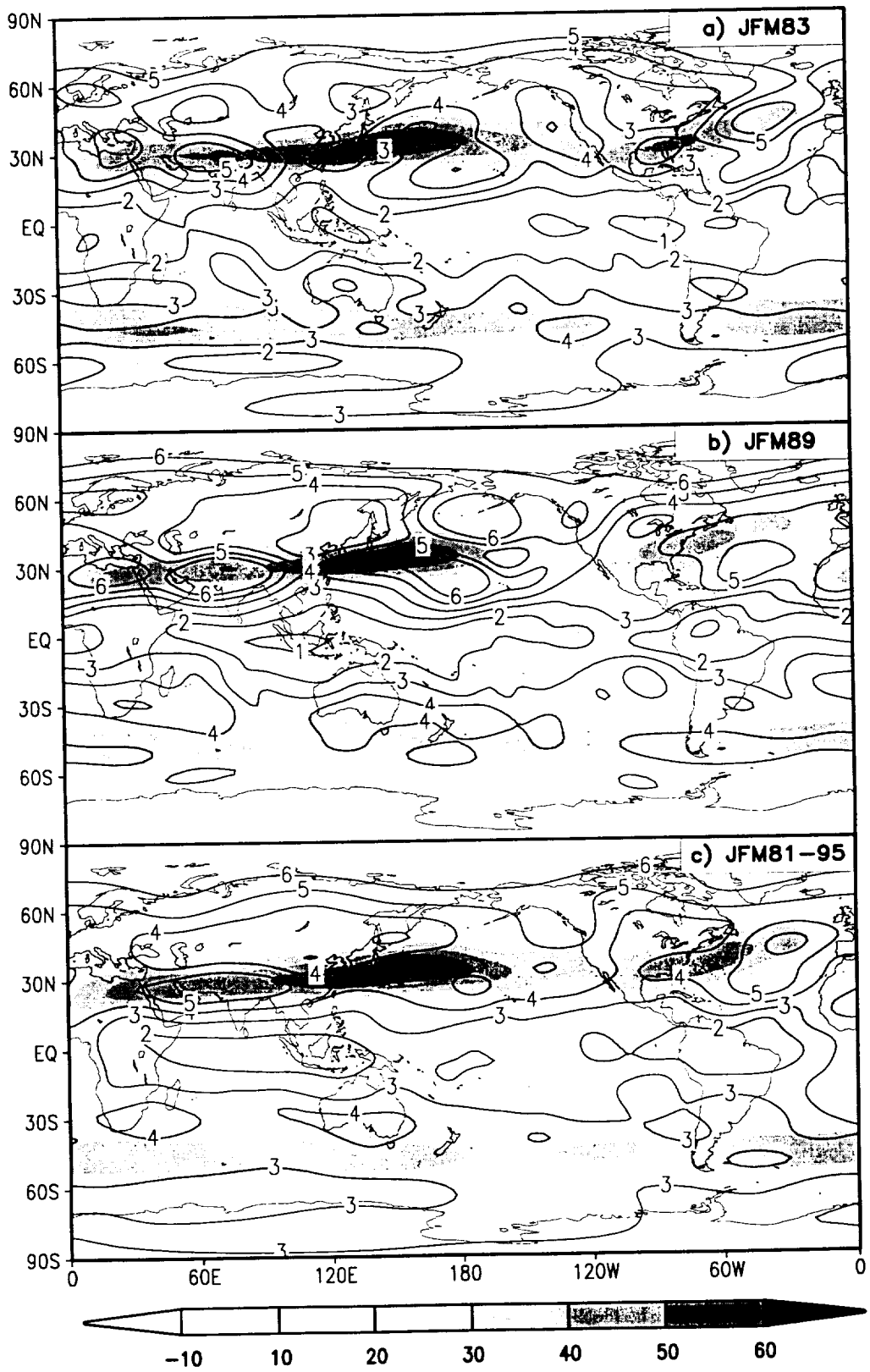

Figure 10: Global distribution of the AGCM JFM ensemble mean 200mb zonal wind (m/s) and the JFM stream function noise (intra-ensemble standard deviation, $m^2/sX10^6$) for a) 1983, b) 1989 and c) 1980-95. The values in c) are based on 9-member ensembles for each year. The 1983 and 1989 values are based on 27 ensemble members.

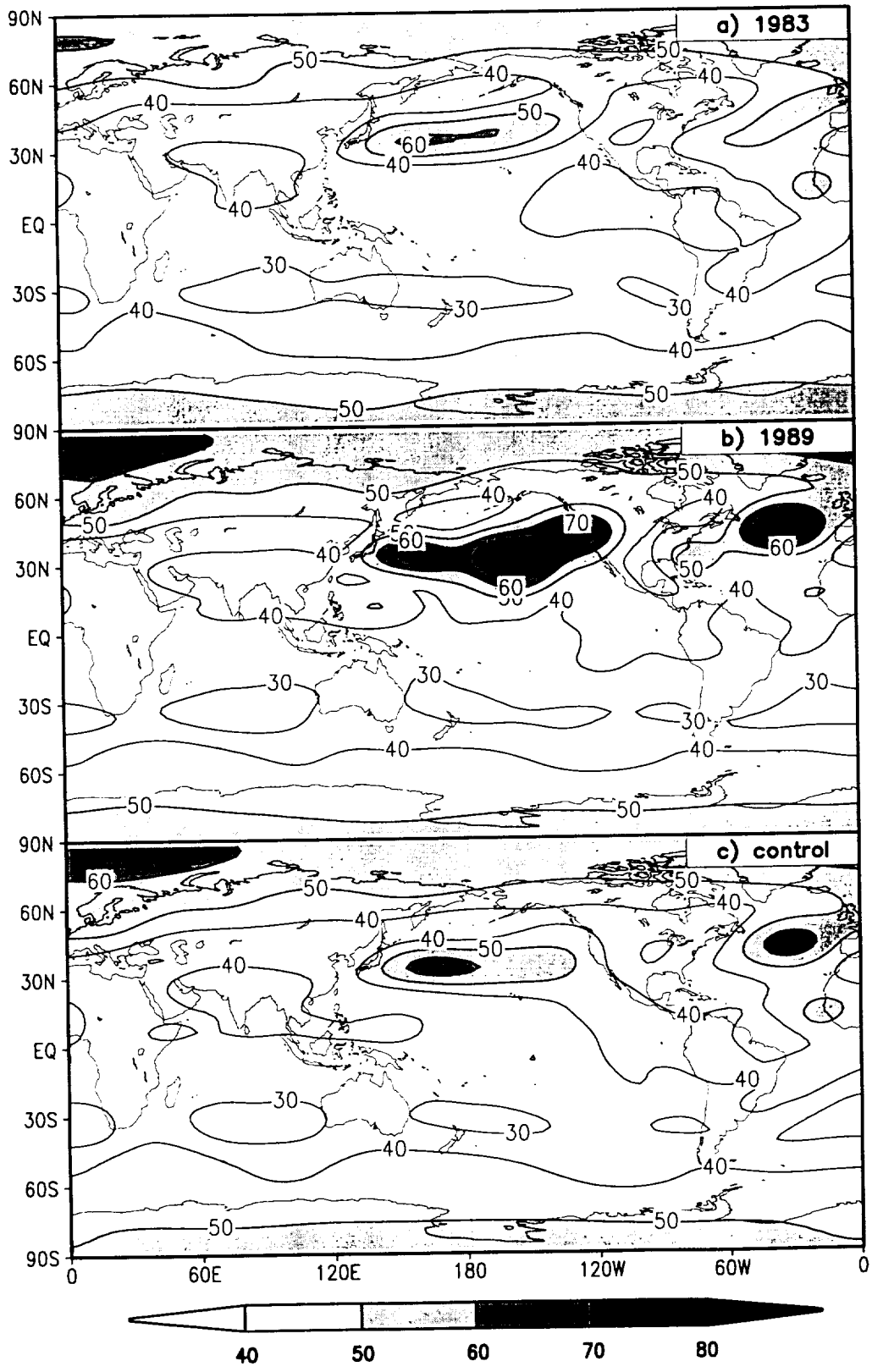

Figure 11: Standard deviation of the stream function from the linear model solutions with global white noise forcing for a) the 1983 base state, b) the 1989 base state, and c) the control (1980-95) base state. Contour intervals are the same in each panel but arbitrary.

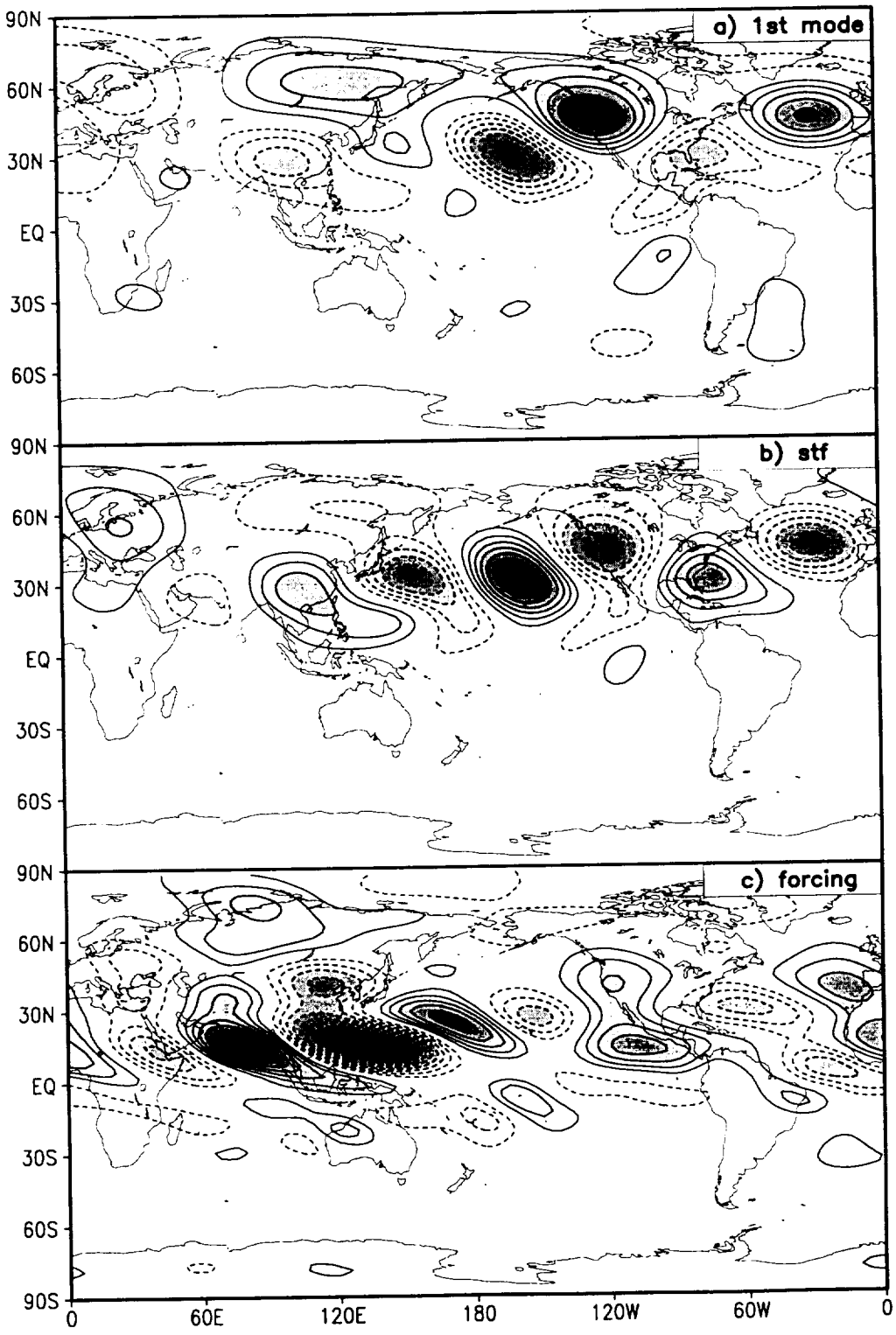

Figure 12: a) The dominant eigenmode of the linear model for the 1989 base state. The dominant SVD of b) the stream function and c) the forcing for the 1989 base state with white noise forcing. Contour intervals are arbitrary.

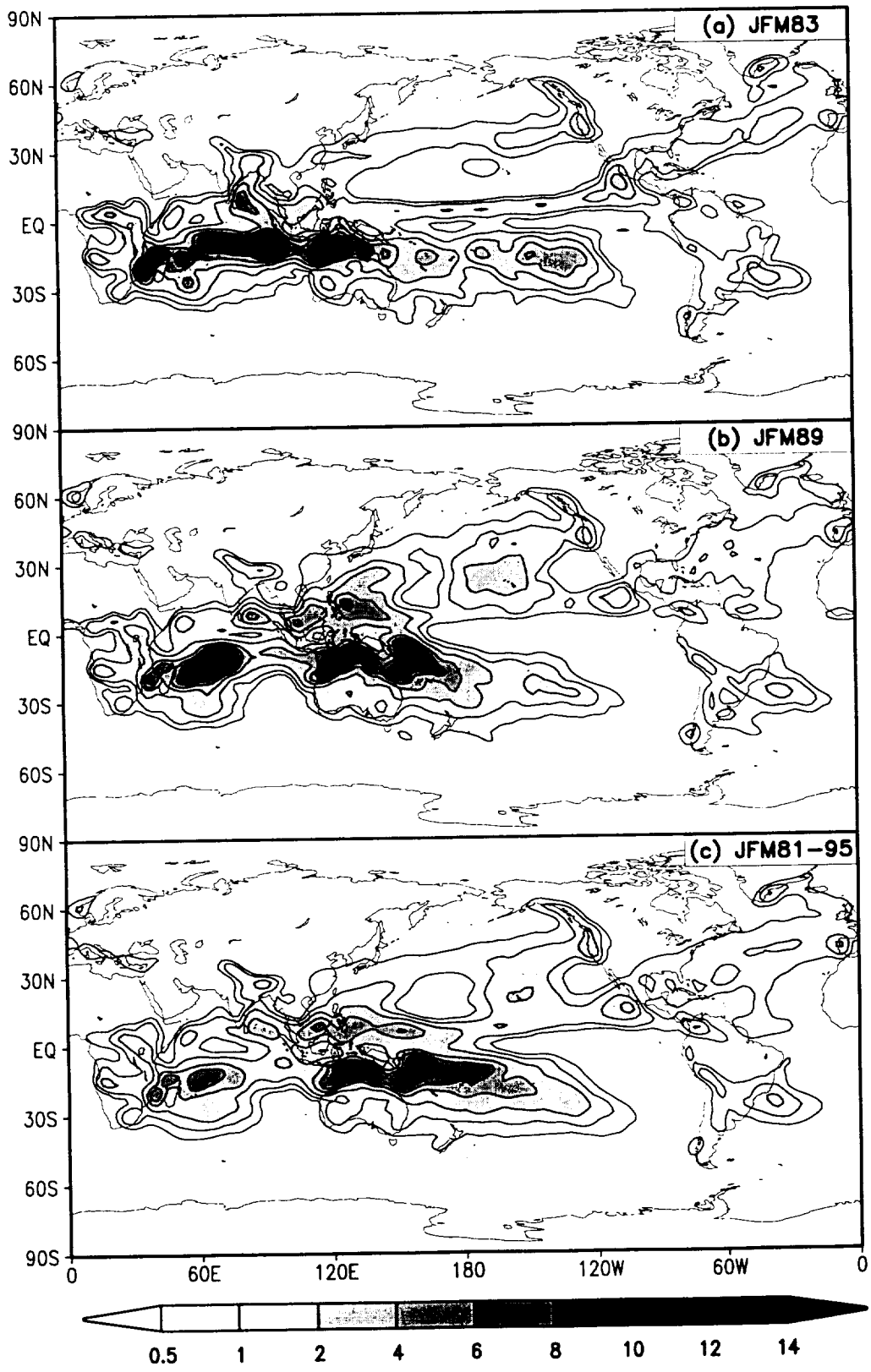

Figure 13: The global distribution of the AGCM noise (intra-ensemble variance) of the JFM precipitation based on a) the 27 ensemble members for 1983, b) the 27 ensemble members for 1989, and c) the 9-member ensembles covering the period 1980-95. Units are $(mm/day)^2$.

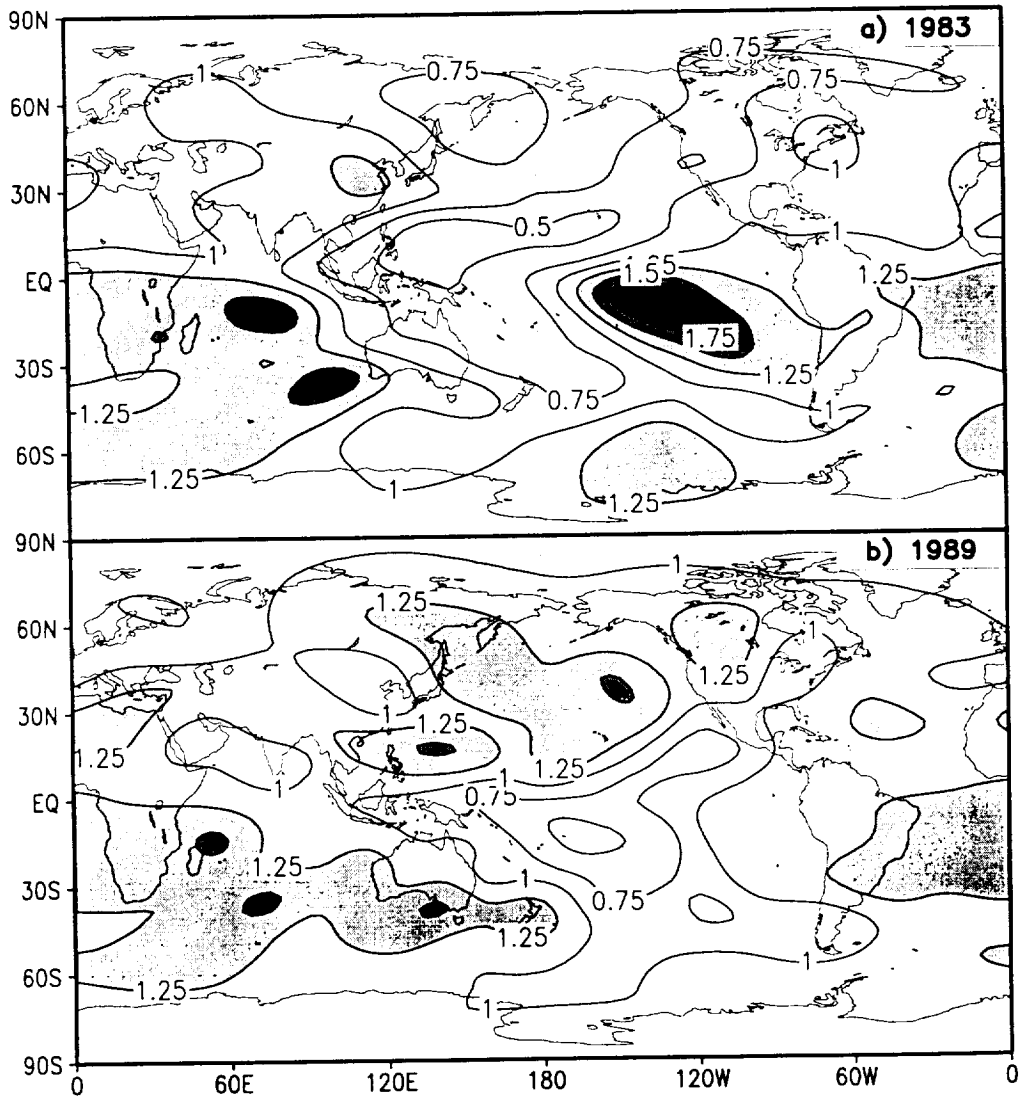

Figure 14: Results from the linear model showing the impact of the AGCM precipitation envelopes applied to the global white noise forcing equatorward of 20°. a) the ratio of the variance of 1983 base state with the 1983 precipitation envelope solutions to the variance of the 1983 base state with the control (1980-95) precipitation envelope solutions. b) the ratio of the variance of 1989 base state with the 1989 precipitation envelope solutions to the variance of the 1989 base state with the control (1980-95) precipitation envelope solutions.

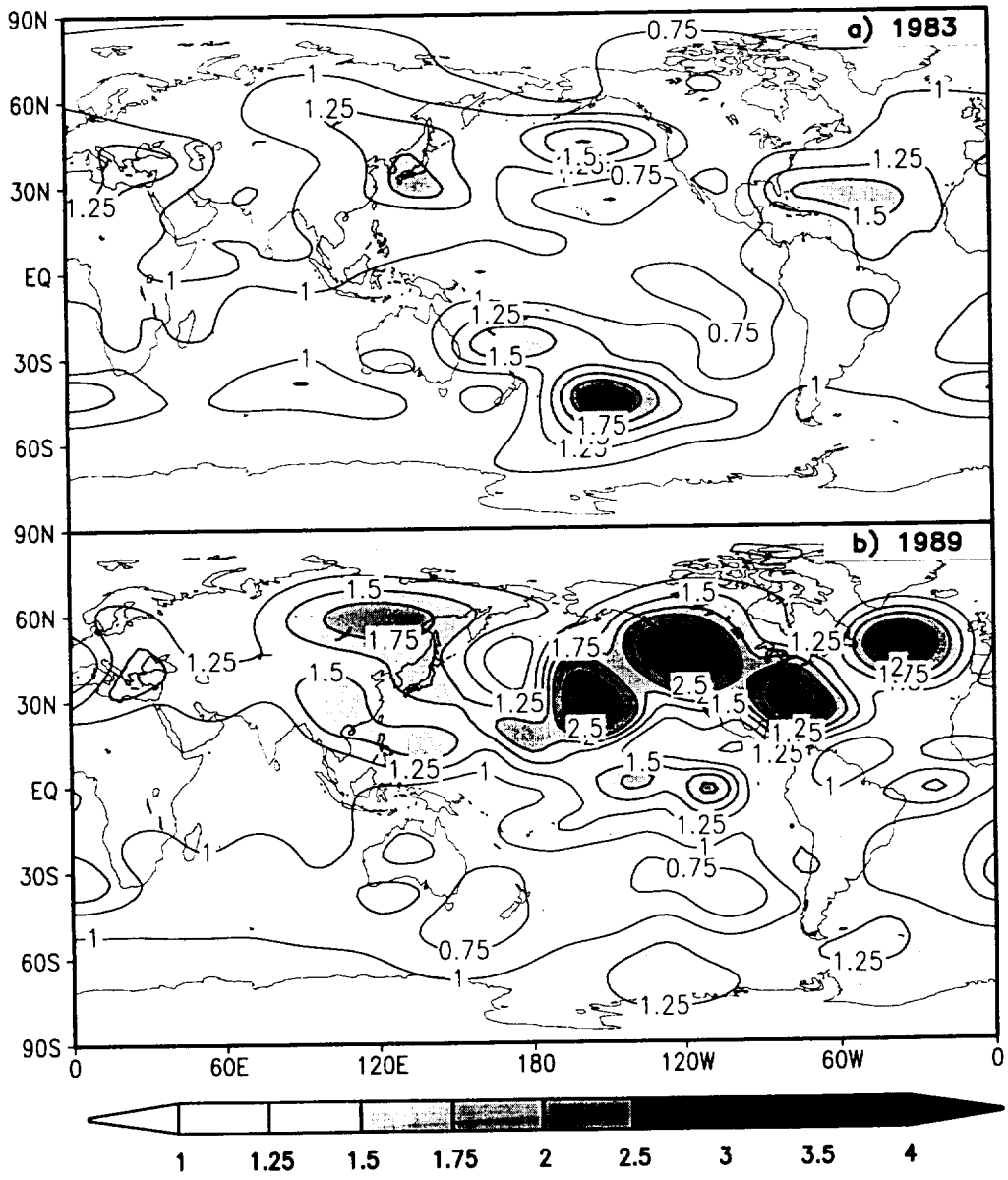

Figure 15: Results from the linear model showing the impact of the AGCM base states. In all runs the AGCM control precipitation envelope is applied to the global white noise forcing equatorward of 20°. See text for details. a) the ratio of the variance of the solutions with the 1983 base state to the variance of the solutions with the control base state. b) the ratio of the variance of the solutions with the 1989 base state to the variance of the solutions with the control base state.

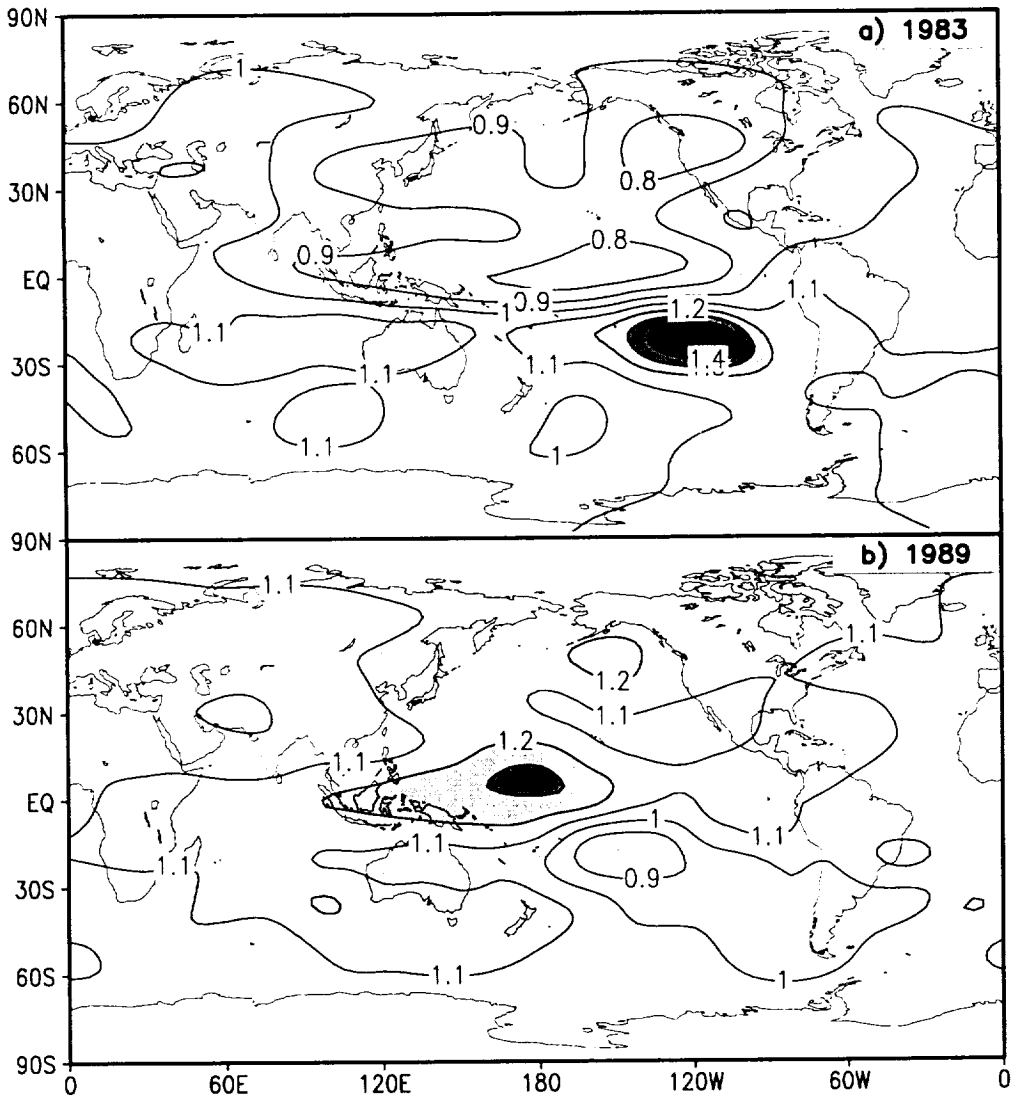

Figure 16: Results from the linear model showing the impact of the AGCM submonthly vorticity flux divergence envelope applied equatorward of 60°. See text for details. a) the ratio of the variance of 1983 base state with the 1983 vorticity flux divergence envelope solutions to the variance of the 1983 base state with the control (1980-95) vorticity flux divergence envelope solutions. b) the ratio of the variance of 1989 base state with the 1989 vorticity flux divergence envelope solutions to the variance of the 1989 base state with the control (1980-95) vorticity flux divergence envelope solutions.